Algal Protein Kinase, Triacylglycerol Accumulation Regulator1, Modulates Cell Viability and Gametogenesis in Carbon/Nitrogen Imbalanced Conditions

Running title: Algal kinase TAR1 modulates C/N-imbalanced responses

Authors: Haruka Shinkawa[1], Masataka Kajikawa[1,*], Yuko Nomura[2], Mayu Ogura[3], Yuri Sawaragi[1], Takashi Yamano[1], Hirofumi Nakagami[2,6], Naoyuki Sugiyama[3], Yasushi Ishihama[3], Yu Kanesaki[4], Hirofumi Yoshikawa[5] and Hideya Fukuzawa[1,*]

[1]Graduate School of Biostudies, Kyoto University, Kyoto 606-8502, Japan

[2]RIKEN Center for Sustainable Resource Science, Kanagawa 230-0045, Japan

[3]Graduate School of Pharmaceutical Science, Kyoto University, Kyoto 606-8501, Japan

[4]NODAI Genome Research Center, Tokyo University of Agriculture, Tokyo 156-8502, Japan

[5]Department of Bioscience, Tokyo University of Agriculture, Tokyo 156-8502, Japan

[6]Present address: Max Planck Institute for Plant Breeding Research, 50829 Cologne, Germany

[*]**Corresponding authors:**

E-mail: fukuzawa@lif.kyoto-u.ac.jp, kajikawa@lif.kyoto-u.ac.jp

Fax: +81-75-753-9228

Abstract

Nutrient-deprived microalgae accumulate triacylglycerol (TAG) in lipid droplets. A dual-specificity tyrosine phosphorylation-regulated kinase, TAG accumulation regulator 1 (TAR1) has been shown to be required for acetate-dependent TAG accumulation and the degradation of chlorophyll and photosynthesis-related proteins in photomixotrophic nitrogen (N)-deficient conditions (Kajikawa et al. 2015). However, this previous report only examined particular condition. Here, we report that in photoautotrophic N-deficient conditions, *tar1-1* cells, with a mutation in the *TAR1* gene, maintained higher levels of cell viability and lower levels of hydrogen peroxide generation and accumulated higher levels of TAG and starch compared with those of wild-type (WT) cells with bubbling of air containing 5% carbon dioxide. Transcriptomic analyses suggested that genes involved in the scavenging of reactive oxygen species are not repressed in *tar1-1* cells. In contrast, the mating efficiency and mRNA levels of key regulatory genes for gametogenesis, *MID*, *MTD*, and *FUS,* were suppressed in *tar1-1* cells. Among the TAR1-dependent phosphopeptides deduced by phosphoproteomic analysis, protein kinases and enzymes related to N assimilation and carbon (C) metabolism are of particular interest. Characterization of these putative downstream factors may elucidate the molecular pathway whereby TAR1 mediates cellular propagation and C and N metabolism in C/N-imbalanced stress conditions.

Footnotes: The nucleotide sequences reported in this paper has been submitted to the DDBJ Sequenced Read Archive under accession number DRA004651. All MS data from the phosphoproteomic analysis are deposited in the Japan Proteome Standard Repository/Database (accession nos. PXD012391 and PXD012311).

Key words: C/N balance; *Chlamydomonas*; dual-specificity tyrosine-phosphorylation-regulated kinase; gametogenesis; hydrogen peroxide; phosphoproteome

Introduction

In eukaryotes, phosphorylation-dependent protein modification plays a major role in the regulation of cell proliferation in stress conditions. Several protein kinases functioning in response to nutrient states are highly conserved as key regulators in eukaryotes, such as AMP-activated protein kinase (AMPK), cyclic AMP-dependent protein kinase A (PKA), and target of rapamycin (TOR) (Shashkova et al. 2015). In plants, SNF1-related kinase 1 (SnRK1), conserved as the plant-specific AMPK family member, is activated when energy storage decreases, due to abiotic stresses such as nutrition depletion (Baena-Gonzalez et al. 2007). Plant TOR and SnRK1 have similar antagonistic roles in different biological processes, including cell division, protein synthesis, reserve accumulation, and autophagy (Hulsmans et al. 2016). Activation of SnRK1 leads to transcriptional reprograming of downstream genes and induces the degradation of proteins, amino acids, lipids, cell walls, starch, and sucrose (Baena-Gonzalez et al. 2007). In yeast, a member of the dual-specificity tyrosine-phosphorylation-regulated kinase (DYRK) family, named Yak1, negatively regulates cell division in glucose-deprivation conditions (Martin et al. 2004, Moriya et al. 2001). TOR negatively regulates Yak1 *via* PKA in glucose-deprivation conditions (Martin et al. 2004). We have reported a positive regulator of acetate assimilation and triacylglycerol (TAG) accumulation, TAG accumulation regulator 1 (TAR1), in photomixotrophic nitrogen (N)-deficient conditions in the model green alga *Chlamydomonas reinhardtii* (Kajikawa et al. 2015). TAR1 phylogenetically belongs to the Yak1-type DYRK family. TAR1 is required for the degradation of both chlorophyll and photosynthesis-related proteins in N-deficient conditions.

When the balance of carbon and nitrogen (C/N) collapses due to N-deficiency, *C. reinhardtii* shows various induced responses, such as degradation of chlorophyll, photosynthesis-related proteins, and chloroplast membrane lipids (Schmollinger et al. 2014,

Siaut et al. 2011), in addition to the accumulation of starch and TAG (Merchant et al. 2012); moreover, cells undergo a phase transition from vegetative cells to gametes (Sager and Granick 1954). It was suggested that excess NADPH and ATP generated by photosynthesis at the early stress stage of N-deficiency are consumed by *de novo* synthesis of starch and fatty acids for integration into TAGs to prevent the redox state in cells from becoming imbalanced (Johnson and Alric et al., 2013). A low-TAG and high-starch accumulation mutant, *pgd1,* shows a decrease in cell viability and an increase in intracellular reactive oxygen species (ROS) compared with wild-type (WT) cells in N-deficient conditions, suggesting that TAG and starch synthesis are involved in the control of the intracellular redox state (Du et al., 2018). In addition to TAR1, another plant-specific DYRK subfamily kinase, STD1, has been reported to negatively regulate TAG accumulation in photoautotrophic N-deficient conditions (Schulz-Raffelt et al. 2016). Based on a phosphoproteomic analysis using the *Chlamydomonas* WT-type strain, STD1 and an AtGRIK1 ortholog phosphatase, called CDPKK2, are suggested to play central roles in the coordination of translational, photosynthetic, proteomic, and metabolomic activity in N-deficient conditions (Roustan et al. 2017).

In photomixotrophic N-deficient conditions, acetic acid is a major organic carbon source for growth in *C. reinhardtii*; acetic acid is utilized mainly to synthesize fatty acids for TAG accumulation (Juergens et al., 2016). In these conditions, the amount of TAG increases in proportion to the concentration of acetic acid in the culture medium (Fan et al. 2012). Conversely, in photoautotrophic N-deficient conditions, the levels of accumulated TAG decrease inversely proportional to increasing levels of supplied CO_2 (Sakurai et al. 2014). The authors hypothesized that the balance between C and N metabolites could be adjusted by decreasing the levels of TAG. Recently, a rapamycin-hypersensitive *C. reinhardtii* mutant called *vip1-1*, in which a gene encoding an inositol hexakisphosphate kinase was disrupted,

was reported to accumulate higher levels of TAG compared with those in WT cells in photomixotrophic conditions (Couso et al. 2016). Because the TAG content in *vip1-1* mutant cells in photoautotrophic conditions was unaffected, suggesting that growth and lipid accumulation with acetic acid as a carbon source in photomixotrophic conditions could be regulated by the TOR kinase and inositol polyphosphate signaling systems.

Although the protein kinase TAR1 plays a positive role in accumulation of TAG in photomixotrophic conditions, its roles in cells in photoautotrophic conditions have not been examined. In order to understand the contribution of TAR1 to cellular responses in photoautotrophic N-deficient conditions, we have characterized a TAR1-defective mutant, *tar1-1*, by analyzing cell viability, generation of hydrogen peroxide (H_2O_2), photosynthetic activity, levels of TAG accumulation, gamete induction, and transcriptomic activity. To further clarify the molecular mechanisms underlying protein phosphorylation by TAR1 and identify possible TAR1-dependent phosphoproteins that are targeted in response to photoautotrophic N-deficiency, we carried out a phosphoproteomic analysis.

Results

Cell viability and accumulation of TAG and starch in the *tar1-1* mutant in photoautotrophic N-deficient conditions

Because changes in supplied CO_2 concentration affect the intracellular C/N balance, algal cells acclimate to C/N-imbalanced stresses by sensing the status of nutrient availability. To evaluate the effects of higher C/N stress on *Chlamydomonas* cells, cell viability and chlorophyll levels of WT and *tar1-1* cells were examined 2 days after transfer from photoautotrophic culture in N-containing medium to N-deficient conditions with continuous bubbling of air containing different CO_2 concentrations (from ambient air containing 0.04–10% CO_2) (Fig. 1A, B). In all the CO_2 conditions tested, the cell viability and chlorophyll

levels of *tar1-1* cells were higher than those of WT cells. To compare CO_2-dependent carbon assimilation between *tar1-1* and WT cells in N-deficient conditions, we measured the levels of total fatty acids constituting TAG molecules (TAG-FA) and starch in the cells cultured with air containing 0.04–10% CO_2 (Fig. 1C, D). Because the cell number per culture and the cell dry weight per cell were not significantly different between WT and *tar1-1* cells when the culture medium was replaced by N-deficient medium (Supplementary Fig. S1A, B), the levels of accumulation of TAG and starch in the cultures 2 days after the transfer to N-deficient conditions were expressed as microgram per milliliter culture. Higher levels of TAG accumulation were observed only in *tar1-1* cells in photoautotrophic N-deficient conditions with bubbling of CO_2-enriched air containing 5% or 10% CO_2 (Fig. 1C). In addition, higher levels of starch accumulation in *tar1-1* cells were observed in photoautotrophic N-deficient conditions aerated with CO_2-enriched air containing 0.5%, 1%, or 5% CO_2 (Fig. 1D).

After 2 days in photoautotrophic N-deficient conditions with CO_2-enriched air containing 5% CO_2 (hereafter referred to as TP–N conditions), *tar1-1* showed pleiotropic phenotypes, such as high levels of viability and accumulation of chlorophyll, TAG, and starch compared with WT cells. Therefore, we focused on time-dependent changes in *tar1-1* cells in TP–N conditions. In contrast to WT and *TAR1*-complemented line (C1) cells, which showed severe chlorosis by day 2, *tar1-1* cells showed markedly less degradation of chlorophyll, resulting in a "stay-green" phenotype (Fig. 2A, B). We measured the time course of cell viability and H_2O_2 content, as representative of ROS, in TP–N conditions. The cell survival rate of the *tar1-1* mutant was 2.2-fold higher than that of WT cells at day 1 (Fig. 2C). On the other hand, the H_2O_2 levels in *tar1-1* cells were 0.27-fold lower than that of WT cells at day 1 in contrast to the rapid accumulation of H_2O_2 in all strains at 6 hours in TP–N conditions (Fig. 2D).

tar1-1 mutant impaired the degradation of photosynthesis-related proteins in TP–N conditions

High-accumulation of carbon products such as TAG and starch was observed in *tar1-1* cells in TP–N conditions. In order to know whether the carbon products were generated by photosynthetically fixed carbon in TP–N conditions, we evaluated the effects of the *tar1* mutation on photosynthesis in TP–N conditions. First, we measured photosynthetic parameters including the maximum quantum efficiency of PS-II (F_v/F_m), quantum efficiency of PS-II photochemistry (ΦII), and maximum rate of photosynthetic oxygen (O_2)-evolution (V_{max}) (Table 1). The F_v/F_m and ΦII values in *tar1-1* cells at day 1 in TP–N conditions (0.49 ± 0.02 and 0.31 ± 0.03, respectively) were significantly higher than those in WT cells (0.27 ± 0.03 and 0.16 ± 0.02, respectively). Although the F_v/F_m and ΦII values in *tar1-1* cells at day 2 fell to 0.27 ± 0.13 and 0.09 ± 0.08, respectively, these values were undetectable in WT and C1 cells. The V_{max} in *tar1-1* cells at day 2 in TP–N condition was 72.4 ± 12 μmol O_2 $mgChl^{-1}$ h^{-1}, whereas it was undetectable at day 2 in WT and C1 cells. These results indicated that *tar1-1* cells could maintain photosynthetic activity for longer than WT cells in TP–N conditions. Second, the cellular levels of photoreaction-related proteins, including the light-harvesting complex protein II (LHCII) in the antenna complex, D1 protein in photosystem II (PsbA), cytochrome *f* in the cytochrome b_6/f complex (PetA), subunit II protein in PS-I (PsaD), and proteins related to the Calvin–Benson cycle, including the large subunit of Rubisco (RbcL), sedoheptulose-1,7-bisphosphate (SBP), phosphoribulokinase (PRK), and glyceraldehyde-3-phosphate dehydrogenase (GAPDH), and chloroplastic glutamyl-tRNA reductase 1 (HemA) for chlorophyll biosynthesis, decreased in *tar1-1* cells, but they were nevertheless all present at higher levels in *tar1-1* cells than in WT and C1 cells (Fig. 3). These results indicated that TAR1 stimulated degradation the photosynthesis-related proteins in TP–N conditions. Although degradation of the cytoplasmic ribosomal protein RPL37 was previously shown in

WT cells in N-deficient conditions (Couso et al., 2018), the cellular levels of RPL37 in *tar1-1* cells decreased as in the case of WT cells in N-deficient conditions (Fig. 3), suggesting that the TAR1 contributes to degrade photosynthesis-related proteins rather than cytoplasmic ribosomal proteins.

tar1-1 cells accumulate high levels of TAG and starch in TP–N conditions

To understand the effect of the *tar1* mutation on changes in the levels of TAG and starch in *tar1-1,* WT, and C1 cells, contents of TAG-FA and starch were time-dependently analyzed after changing the C/N balance from TP+N to TP–N conditions (Fig. 4A, B). Although the amounts of TAG-FA both in *tar1-1* and WT cells increased to approximately 3 μg ml^{-1} at 1 day (Fig. 4A), the level of TAG-FA accumulation in *tar1-1* cells (5.3 ± 0.4 μg ml^{-1}) at day 2 was 1.7-fold higher than that in WT cells (3.2 ± 1.0 μg ml^{-1}) (Fig. 4A). Similarly, although at day 1, the starch contents both in *tar1-1* and WT reached approximately 200 μg ml^{-1}, at day 2 starch accumulation in *tar1-1* cells was 352.9 ± 28.8 μg ml^{-1}, which was 1.6-fold higher than in WT cells (218.7 ± 34.2 μg ml^{-1}) (Fig. 4B). After 2 days, TAG and starch levels in *tar1-1* cells reached a plateau that was sustained for the rest of the assay period of 4 days.

The fatty acid compositions of TAG in *tar1-1* at day 2 in TP–N conditions were compared with those in WT in the same conditions. The relative abundances of 16:1Δ^{9}, 16:2$\Delta^{7,10}$, 16:3$\Delta^{4,7,10}$, 18:1Δ^{9}, 18:1Δ^{11}, and 18:2$\Delta^{9,12}$ in TAG of *tar1-1* cells were significantly higher than those in WT cells. On the other hand, the proportions of 16:0, 16:3$\Delta^{7,10,13}$, 18:0, 18:3$\Delta^{5,9,12}$, and 18:3$\Delta^{9,12,15}$ in TAG of *tar1-1* cells were significantly lower than those in WT cells (Supplementary Fig. S2). The *tar1-1* cells accumulated greater amounts of membrane lipids than WT cells; these included sulfoquinovosyl diacylglycerol (SQDG), digalactosyldiacylglycerol (DGDG), phosphatidylinositol (PI), diacylglycerol-*N*, *N*, *N*-trimethylhomoserine (DGTS), and phosphatidylethanolamine (PE) (Fig. 4C). Laser scanning

confocal microscopic and transmission electron microscopic observations revealed that lipid droplets and starch granules were more developed in *tar1-1* than WT cells (Supplementary Fig. S3). Higher levels of accumulation of starch and TAG could lead to increases in biomass in *tar1-1* cells. Actually, the dry weight of single cells (0.27 ng ± 0.029 $cell^{-1}$; Supplementary Fig. S1B) and cell size (7.4 μm; Supplementary Fig. S1C) of the *tar1-1* mutant were 1.8-fold and 1.3-fold greater than those of WT cells (cell dry weight: 0.15 ng ± 0.005 $cell^{-1}$, cell size: 5.5 μm) at day 2 in TP–N conditions, although the cell densities, expressed as "cells ml^{-1} culture", both of *tar1-1* and WT cells did not change significantly in TP–N conditions (Supplementary Fig. S1A). All of the physiological phenotypes of *tar1-1* cells analyzed above were restored to WT levels in the C1 line in TP–N conditions, consistent with the analysis of photomixotrophic growth conditions reported previously (Kajikawa et al. 2015).

Decreased mating efficiency and expression levels of gametogenesis-related genes in the *tar1-1* mutant

Because the mutation in the *TAR1* gene leads to the maintenance of cell viability and photosynthetic activity even in TP−N conditions, disruption of *TAR1* seems more advantageous for the survival of *C. reinhardtii* cells in TP−N conditions. Given this apparent advantage of the mutation, we wondered if there was also a downside, and we asked whether the mutation impacted other cellular functions, such as mating efficiency. In order to clarify whether the *tar1* mutation affected gametogenesis of *Chlamydomonas* cells, mating efficiencies of *tar1-1* (mating type minus; mt^-) and a mt^+-type progeny of *tar1-1*, named *tar1-1*-F2-11 (mt^+) were examined. In contrast to the mating efficiencies of WT (C9, mt^-) × WT (CC-125, mt^+) and C1 (mt^-) × WT (CC-125, mt^+), which were 53% and 42%, respectively, those of *tar1-1* (mt^-) × WT (CC-125, mt^+), *tar1-1*-F2-11 (mt^+) ×WT (C9, mt^-), and *tar1-1* (mt^-) × *tar1-1*-F2-11 (mt^+) were significantly lower (5.8%, 2.1%, and 1.3%, respectively) than

that of WT (mt^-) × WT (mt^+) (Fig. 5A).

The relative mRNA levels of a master regulator of gametogenesis in the mt^- gamete, *MID* (Ferris and Goodenough 1997), were lower in the *tar1-1* mutant than those in WT and C1 cells, both at 0 and 2 h after the start of N-deficiency treatment (Fig. 5B). The expression levels of *MTD* and *GSM* also decreased to 15% and 16% in *tar 1-1* cells compared with WT cells after 2 h of N-deficiency (Fig. 5B). The expression levels of *FUS* and *SAG* in gametogenesis of mt^+ gametes of *tar1-1*-F2-11 also decreased to 9.5% and 21%, respectively, compared with that of WT (CC-125, mt^+), at 2 h of N-deficiency.

Differentially expressed genes regulated by TAR1 in TP–N and TAP–N conditions

As assessed using quantitative RT-PCR, the mRNA abundance of *TAR1* itself did not change in response to C/N-imbalance (Supplementary Fig. S4). To find genes whose mRNA abundances were affected by the loss of TAR1, differentially expressed genes (DEGs) were estimated by comparison of RNA-seq data obtained from *tar1-1*, WT, and C1 cells in TP+N conditions, and 6 h after the transfer of cells from the TP+N to TP–N conditions using the DEseq algorithm with a statistical q-value cutoff <0.05 (Anders and Huber, 2010, Supplementary Table S1; Supplementary Dataset S1). Furthermore, *tar1-1* accumulates higher levels of TAG and starch compared with WT and C1 specifically in TP–N conditions (in this study) in contrast to low-TAG accumulating phenotypes of *tar1-1* in TAP–N conditions (Kajikawa et al. 2015). To reveal the differences in gene expression patterns regulated by TAR1 between photoautotrophic and photomixotrophic conditions, we compared RNA-seq data between TP–N conditions (this study, Supplementary Dataset S1) and those in the TAP–N conditions (Kajikawa et al. 2015; Supplementary Dataset S2).

Among the DEGs in TP–N or TAP–N conditions, we classified the DEGs into up-

regulated DEGs in WT, C1, and *tar1-1* cells compared with TP+N or TAP+N conditions or down-regulated DEGs (Supplementary Fig. S5, Kajikawa et al., 2015). The RNA-seq analysis showed that DEGs in WT and C1 lines did not overlap with each other completely. These differences in gene expression pattern between WT and C1 might be caused by other mutation(s) other than the *tar1* insertional mutation occurring during transformation of the plasmid DNA encoding the *TAR1* gene into *tar1-1* cells. Therefore, DEGs overlapping between WT and C1 were used as control DEGs.

Among DEGs in TP–N conditions, a total 218 genes were up-regulated in both WT and C1 cells (left Venn diagram in Fig. 6A). Comparing mRNA abundances in *tar1-1* with those in WT and C1 cells cultured in TP–N conditions, the mRNA abundances of 351 DEGs were significantly higher (left Venn diagram in Fig. 6A). Among these, 80 overlapping DEGs were *TAR1*-dependent up-regulated genes in TP–N conditions. RNA-seq data in TAP–N conditions were processed similarly (right Venn diagram in Fig. 6A). Consequently, 60 DEGs were shown to be *TAR1*-dependent up-regulated genes in TAP–N conditions. Twenty-nine DEGs that overlapped between TP–N and TAP–N conditions were defined as 'DEGs whose expression levels were up-regulated *TAR1*-dependently in common in N-deficient conditions' [group (a) in the middle of the Venn diagram in Fig. 6A, Supplementary Dataset S3. TAR1-dependent genes specifically expressed in TP–N or TAP–N conditions were found to include 51 and 31 DEGs and defined as 'DEGs whose expressions levels were up-regulated *TAR1*-dependently in TP–N or TAP–N conditions specifically', [groups (b) and (c) in the middle of the Venn diagram in Fig. 6A, Supplementary Dataset S4 and S5, respectively]. Gene ontology (GO)-enrichment analysis revealed that genes encoding metabolic enzymes related to the urea cycle and amino acid synthesis; argininosuccinate lyase (*ARG7*), carbamoyl phosphate synthase, small subunit (*CMP2*), argininosuccinate synthase (*AGS1*), and ornithine carbamoyltransferase (*OTC1*), were significantly enriched in the group (a) as a GO Slim term

‘Cellular amino acid metabolic process’ [Supplementary Fig. S6A (a), Supplementary Table S2]. Furthermore, urate and purines transporter, Xanthine/uracil/vitamin C permease-like (*UAPA6*) and cationic amino acid transporter (*AOC5*) were also significantly enriched in this group (a) as a GO Slim term ‘Transmembrane transporter activity’ [Supplementary Fig. S6A (a), Supplementary Table S2].

Similarly, a total 180 DEGs overlapping between TP–N and TAP–N conditions were defined as ‘DEGs whose expression levels were increased by *tar1* disruption in common in N-deficient conditions’ [group (d) in the middle of the Venn diagram in Fig. 6B, Supplementary Dataset S6]. The 124 and 131 DEGs were defined as ‘DEGs whose expression levels were increased by *tar1* disruption in TP–N or TAP–N conditions specifically’, respectively [groups (e) and (f) in the middle of the Venn diagram in Fig. 6B, Supplementary Dataset S7 and S8, respectively]. Among the DEGs in group (d), six genes encoding amino acid tRNA ligases, including methionine-tRNA ligase (*TSM1*), alanine-tRNA ligase (*TSA1*), leucine-tRNA ligase, bifunctional glutamate/proline-tRNA ligase, valine-tRNA ligase (*TSV*), and isoleucyl-tRNA ligase (*TSI*) were significantly enriched as ‘tRNA metabolic process’ genes [Supplementary Fig. S6B (d), Supplementary Table S3]. Moreover, in the group (e), such as those encoding alternative oxidase (*PTO1*) and glutathione peroxidase (*GPX5*) involved in the scavenging of ROS, thioredoxin h2 (*TRXh2*) in protection against ROS, and Assimilatory sulfite reductase (ferredoxin) / Sulfite reductase (ferredoxin), gamma-butyrobetaine hydroxylase-related, and peptide-methionine (R)-S-oxide reductase involved in the redox reaction were significantly enriched as ‘Oxidoreductase activity’ [Supplementary Fig. S6B (e), Supplementary Table S3].

Total 24 DEGs overlapped between TP–N and TAP–N conditions were defined as ‘DEGs whose expression levels were down-regulated *TAR1*-dependently in common in N-deficient conditions’, in which the GO Slim term ‘tRNA metabolic process’ including serine-

tRNA ligase (*SERRS2*), aspartate-tRNA ligase (*TSD2*), valine-tRNA ligase (*TSV*), bifunctional glutamate/proline-tRNA ligase, tryptophan-tRNA ligase (*TSW1*) was significantly enriched [group (g) in the middle of the Venn diagram in Fig. 6C, Supplementary Fig. S6C (g), Supplementary Dataset S9, Supplementary Table S4]. TAR1-dependent DEGs found specifically in TP–N or TAP–N conditions in Fig. 6C were defined as 'DEGs whose expression levels were down-regulated *TAR1*-dependently in TP–N or TAP–N conditions specifically' consisted of 36 and 23 genes, respectively [groups (h) and (i) in the middle of the Venn diagram in Fig. 6C, Supplementary Dataset S10 and S11, respectively].

In group (h), the GO Slim term 'Photosynthesis' consisted of photosystem-related genes, such as photosystem I reaction center subunit N (*PSAN*), PSII-associated chlorophyll a/b-binding protein (*LHCBM4*), and Oxygen-evolving enhancer protein 2 (*PSBP1*), were significantly enriched [Supplementary Fig. S6C (h), Supplementary Table S4]. On the other hand, in group (i), the GO Slim term 'Cofactor metabolic process', including tetrapyrrole-biosynthesis-related genes encoding magnesium-chelatase subunit chlD (*CHLD*), magnesium-chelatase subunit chlI (*CHLI1*), and uroporphyrinogen-III decarboxylase (*UPD1*), were significantly enriched [Supplementary Fig. S6C (i), Supplementary Table S4].

A total 31 DEGs overlapping between TP–N and TAP–N conditions were defined as 'DEGs whose expression levels were decreased by *tar1* disruption in common in N-deficient conditions' [group (j) in the middle of the Venn diagram in Fig. 6D, Supplementary Dataset S12]. TAR1-dependent DEGs found specifically in TP–N or TAP–N conditions were defined as 'DEGs whose expression levels were decreased by *tar1* disruption in TP–N conditions specifically'. A total 126 and 34 DEGs were classified in these categories, respectively [groups (k) and (i) in the middle of the Venn diagram in Fig. 6D, Supplementary Dataset S13 and S14]. In group (k), the GO Slim term 'Carbohydrate metabolic process' consisting of three TCA cycle-related genes: NAD-dependent malate dehydrogenase (*MDH1*), malate

synthase (*MAS1*), and isocitrate dehydrogenase (*IDH2*); and three Calvin cycle related genes encoding sedoheptulose-1,7-bisphosphatase (*SEBP1*), fructose-1,6-bisphosphate aldolase 1 (*FBA3*), and glyceraldehyde 3-phosphate dehydrogenase A (*GAP3*); and two glycolysis/gluconeogenesis pathway-related genes encoding enolase (*PGH1*), and pyruvate kinase (*PYK1*) were significantly enriched [Supplementary Fig. S6D (k), Supplementary Table S5]. Moreover, in group (k), the GO Slim term 'Oxidoreductase activity' consisted of genes for redox-dependent enzymes, such as *GAP3*, *IDH2*, *MDH1*, glutamate synthase ferredoxin-dependent (GSF1), ferredoxin-NADP reductase (*FNR1*), and thioredoxin f1 (*TRX f1*), was also significantly enriched (Supplementary Table S5).

Based on RNA-seq analyses, TAR1 was necessary to increase the mRNA levels of genes related to N-assimilation, including urea cycle enzymes and transporters of N-containing compounds, and also to decrease the mRNA levels of genes encoding amino acids tRNA ligases in N-deficient conditions regardless of the presence or absence of acetic acid. On the other hand, specifically in TP–N conditions, the *tar1* mutation caused the expression of several genes involved in responses to ROS, and decreased mRNA abundance of several genes such as *FNR1* and *TRX f1* related to the regulation of redox state, and other enzymatic genes related to carbon metabolism regulated by redox state.

In vitro protein phosphorylation by a partial TAR1 containing the kinase domain

To identify putative target proteins of TAR1-mediated phosphorylation in *C. reinhardtii* cells in TP–N and TP+N conditions, we initially tried to express full-length TAR1 recombinant protein in *Escherichia coli* but this was not successful. Therefore, a partial TAR1 recombinant protein (pTAR1; Thr-421 to Leu-859), containing the kinase domain (Val-495 to Ile-830) and a partial TAR1 recombinant protein with a K523R substitution at the putative phosphate

anchor site as a kinase-dead (KD) mutant (pTAR1^{KD}) (Kajikawa et al. 2015), were used for *in vitro* assays with [γ-^{32}P]- ATP (Supplementary Fig. S7). pTAR1 showed prominent transphosphorylation activity with several endogenous proteins extracted from cells cultured in TP–N and TP+N conditions (lanes 1, 4 in Supplementary Fig. S7). By contrast, pTAR1^{KD} did not show any phosphorylation activity (lanes 2, 5 in Supplementary Fig. S7). The amounts of phosphopeptides in the *in vitro* reaction with non-radiolabeled ATP were evaluated by quantitative liquid chromatography–tandem mass spectrometry (LC-MS/MS) analysis using stable-isotope dimethyl labeling. Starting with total proteins from cells cultured in TP–N conditions, peptides were prepared from either the pTAR1-mediated reaction, and labeled with a heavy isotope tag (H), or the pTAR1^{KD} reaction, and labeled with a light isotope tag (L). Taking a two-fold difference in H/L ratio as the threshold, 538 phosphopeptides appeared with higher abundance in pTAR1-mediated reactions than in pTAR1^{KD}-mediated reactions. For comparison, 520 phosphopeptides appeared with higher abundance in pTAR1-treated reactions with total proteins from cells grown in the TP+N conditions than in pTAR1^{KD}-treated reactions with total proteins from cells grown in the same conditions. Taken together, a total of 785 nonredundant phosphopeptides (462 phosphoproteins) were obtained as *in vitro* phosphorylated proteins by pTAR1 (Supplementary Dataset S15). These phosphopeptides were phosphorylated at serine, threonine, and/or tyrosine residues (Supplementary Dataset S15).

Phosphoproteomic analysis of *tar1-1* in TP–N conditions

In order to reveal TAR1-dependent changes in protein phosphorylation during the transition response to TP–N conditions, phosphopeptides derived from *tar1-1*, WT, and C1 cells in TP–N (6 h after transfer) and TP+N (control) conditions were analyzed (Supplementary Dataset S16). In total, 5,251 putative phosphopeptides were identified. Of these, 947 in WT, 307 in *tar*

1-1, and 550 in C1 lines showed significant increases (p value < 0.05) in abundance after 6 h in TP–N, relative to TP+N conditions (Supplementary Fig. S8A). On the other hand, the respective numbers of phosphopeptides whose ion intensity decreased significantly after 6 h in TP–N compared with TP+N conditions, were 1,069 in WT, 1,889 in *tar1-1*, and 1,864 in C1 lines, respectively (Supplementary Fig. S8B). Among these phosphopeptides, the phosphopeptides were classified into four groups by expression patterns (Fig. 7A-D) to find phosphopeptides whose differential ion intensity was significantly changed by the mutation of the *tar1* gene. Because the ion intensities of 222 phosphopeptides were up-regulated *TAR1*-dependently in TP–N conditions, those peptides were assumed to be candidate TAR1-dependent phosphoproteins and defied as 'phosphopeptides whose intensities were up-regulated *TAR1*-dependently in TP–N conditions' (Fig.7A, Supplementary Dataset S17). To narrow down the TAR1-dependent phosphoproteins, phosphoproteins, whose phosphosite(s) were consistent with those of phosphosite(s) derived from the phosphoproteomic analysis *in vitro* (Supplementary Dataset S15), were selected. This set consisted of the following phosphoproteins: two protein kinases, calcium-dependent protein kinase 11 (CDPK11) and mitogen-activated protein kinase kinase kinase (MLTK); three metabolic enzymes, glutamine synthetase, carnosine synthase, ammonium transporter 4 (AMT4) involved N-assimilation, and phosphofructokinase 1 (PFK1) in carbon metabolism (Table 2).

In case of other expression pattern groups, the ion intensity of a total of 139 phosphopeptides increased in *tar1-1* cells after transfer to the TP–N conditions and also higher in *tar1-1* than WT and C1 in the TP–N condition (Fig. 7B, Supplementary Dataset S18). These phosphopeptides were defied as 'phosphopeptides whose intensities increased by *tar1*-disruption in TP–N condition'. On the other hand, the ion intensity of 107 phosphopeptides decreased in WT and C1 lines after transfer to TP–N and also was lower in WT and C1 compared with *tar1-1* (Fig. 7C, Supplementary Dataset S19). We defined these

phosphopeptides as ‘phosphopeptides whose intensities were down-regulated *TAR1*-dependently in TP–N condition’. In contrast, the ion intensity of 507 phosphopeptides decreased in *tar1-1* cells after transfer to the TP–N condition and also was lower in *tar1-1* than WT and C1 in the TP–N conditions (Fig. 7D, Supplementary Dataset S20). We defined these phosphopeptides as ‘phosphopeptides whose intensities were decreased by *tar1*-disruption in TP–N conditions’.

To further characterize these TAR1-dependent phosphoproteins, GO-enrichment analysis was performed. Consequently, 9 GO Slim terms category were enriched in phosphopeptides whose intensities were increased by *tar1*-disruption in TP–N conditions (in Fig. 7D), but no GO Slim terms were enriched in the other three groups (Fig. 7E, Supplementary Table S6). The term “Cellular protein modification process” was significantly enriched in group E (Fig. 7E and Supplementary Table S6). The phosphoproteins assigned to the term ‘protein modification process’ in group E included: protein kinases involved in the mitogen-activated protein kinase (MAPK) cascade, such as MAPK3, MAPK4, MAPK7, MAPK8, myosin light chain kinase (MLCK1), MAP kinase kinase kinase (MEKK), and four protein phosphatases, protein phosphatase 2C3 (PP2C3), PP2C4, phosphoprotein phosphatase 10 (PPP10) and PPP16 (Supplementary Table S6).

Discussion

Generation of ROS and chlorosis mediated by TAR1

In contrast to WT cells, which showed loss of cell viability in photoautotrophic N-deficient conditions, *tar1-1* cells showed significantly higher cell viability than the WT cells (Fig. 1A and Fig. 2). In contrast of that, both *tar1-1* and WT cells kept high levels of cell viability (≥ 90%) during 6 days in photomixotrophic TAP–N conditions (Kajikawa et al. 2015). This means that the absence of acetate and supply of CO_2-enriched air to the cells drastically

affects the fate of cell viability in the WT cells but not in *tar1-1* cells. After the transfer of cells to TP–N conditions, the level of H_2O_2 in both strains increased initially until 6 hours, but the level of H_2O_2 in *tar1-1* cells was significantly lower than that in WT cells at day 1 (Fig. 2D), and cell viability was maintained for 4 days in TP–N conditions, unlike WT cells (Fig. 2C). It was reported that accumulated TAG may protect cells against oxidative damage in N-deficient conditions by consuming a large proportion of accumulated NADPH derived from photosynthesis and by limiting the generation of ROS (Li et al. 2012, Johnson and Alric 2013). In *tar1-1* cells, the mRNA abundances of *PTO1* and *GPX5* involved in scavenging of ROS and a homolog of *TRXh1*, *TRXh2*, involved in DNA repair (Sarkar et al., 2005), increased in *tar1-1* cells (Supplementary Dataset S7). The expression of these genes for the ROS-scavenging system is reported to be induced by exogenous H_2O_2 treatment (Blaby et al., 2015), and activation of ROS-scavenging systems contributed to the maintenance of higher levels of cell viability, in addition to TAG accumulation (Du et al., 2018). On the other hand, ROS are known to function as signaling molecules in response to abiotic and biotic stresses in plants and microalgae (Pérez-Pérez et al. 2012, Shao et al. 2013, Baxter et al. 2014). In *C. reinhardtii* WT cells, a temporary increase in H_2O_2 approximately 1 day after transfer to TP–N conditions could be a signal to induce chlorosis and proteolysis in C/N-imbalanced stress conditions.

TAR1 down-regulates photosynthesis by degrading photosynthesis-related proteins

In N-deficient conditions, microalgae inhibit photosynthetic-related protein production and decrease photosynthetic activity by degrading chlorophyll, chloroplast membranes (Sakurai et al., 2014), photosynthesis-related proteins (Wei et al., 2014), and cytoplasmic and chloroplastic ribosomal proteins (Schmollinger et al. 2014). We reported previously that *tar1-*

1 cells maintained their chlorophyll content and photosynthetic-related protein production, such as RbcL and PetA, compared with WT cells in TAP−N conditions (Kajikawa et al. 2015). Similarly, in *tar1-1* cells, the rate of degradation of the photosynthetic apparatus was slower than that in WT and C1 cells in TP–N conditions (Fig. 3), suggesting that TAR1 kinase could mediate these protein degradation mechanisms, possibly *via* protein phosphorylation in either case of photomixotrophic and photoautotrophic N-deficient conditions. Wei et al. (2014) reported that the chloroplast proteases FtsH and Clp are involved in degradation of the cytochrome b_6/f complex and Rubisco. On the other hand, RNA-seq and phosphoproteomic analysis in this study showed that the mRNA abundance of *FtsH* and *Clp* and the intensity of phosphopeptides derived from FtsH and Clp proteins were not affected by the *tar1* mutation. Therefore, it is possible that other chloroplast-degrading systems such as autophagy, as reported in *Arabidopsis*, could be functioning and regulated by TAR1 in WT *Chlamydomonas* cells (Ishida et al. 2008, Kajikawa et al. 2018).

Previously, it was suggested that the amount and activity of PS-II proteins decrease in comparison with those of PS-I in *C. reinhardtii* cells in N-deficient conditions (Plumley and Schmidt, 1989, Juergens *et al*., 2015). Actually, in WT and C1 cells in TP–N conditions, F_v/F_m, ΦII values, and V_{max} decreased rapidly and became undetectable by day 2 (Table 1). It is well known that the reaction center protein D1 (PsbA) in PS-II has a relatively rapid turnover rate with an effective degradation system as part of the PS-II repair cycle (Aro *et al*. 1993), in which protein phosphorylation plays an important role (Tikkanen and Aro, 2012; Kato and Sakamoto, 2014). On the other hand, PS-I is more robust in normal light conditions. However, immunoblotting analysis in this study suggested that both PS-II and PS-I subunits are degraded rapidly in WT cells in highly C/N-imbalanced conditions. In the *tar1-1* mutant, the amount of the PS-I protein PsaD did not decrease, whereas the amount of the PS-II protein PsbA decreased up to day 2 in TP−N conditions (Fig. 3). These results suggested that the

specific degradation system for PS-II is functional even in *tar1-1*, whereas the *tar1* mutation delayed the degradation of the PsbA or increased the recycling rate of PsbA, leading to the maintenance higher O_2-evolving activity in *tar1-1* cells. Altogether, TAR1 is also involved in the more general protein degradation system that affects not only photosystem proteins but also the other chloroplast components in TP−N conditions.

In contrast to plastidic photosynthesis-related proteins, degradation of the cytoplasmic protein RPL37 in TP−N conditions was not affected by the *tar1-1* mutation (Fig. 3). In considering that the degradation of RPL37 protein after N-deficiency was inhibited by treatment with an autophagy inhibitor, Concanamycin A, but not a proteasome inhibitor, MG132 (Couso et al. 2016), it could be possible that autophagic pathway may be involved in the degradation of cytoplasmic ribosomal proteins, whereas TAR1 mainly contributes to the degradation of chloroplast proteins.

TAR1 functions as a negative regulator of TAG and starch accumulation in TP–N conditions

Previously, *tar1-1* was isolated as a low-TAG accumulation mutant in photomixotrophic N-deficient conditions (Kajikawa et al. 2015). In contrast, *tar1-1* cells surpassed WT cells in the amounts of TAG, starch, and dry mass of cells per culture at day 2 in TP–N conditions (Fig. 1C, D, Fig. 4A, B and Supplementary Fig. 1B). Why does the function of TAR1 appear opposite between mixotrophic and photoautotrophic conditions? In mixotrophic N-deficient conditions, starch is predominantly synthesized using photosynthetically fixed carbon, whereas more than 75% of fatty acids are produced from exogenous acetate (Juergens et al., 2016). We reported previously that consumption rate of acetate in the culture medium with *tar1-1* cells was slower than that with WT cells, implying that acetate supply for *de novo* synthesis of TAG was defective in the *tar1-1* mutant in photomixotrophic N-deficient

conditions (Kajikawa et al., 2015). Recently, Couso et al. (2016) reported that a *vip1-1* mutant accumulated higher-levels of TAG and also showed hyper-sensitivity to rapamycin specifically in photomixotrophic conditions. The gene responsible for the *vip1-1* mutant is an inositol hexakisphosphate kinase of the VIP family, suggesting that rapamycin-dependent growth suppression and lipid accumulation are regulated by TOR kinase and inositol polyphosphate signaling systems. In budding yeast, TOR negatively regulates Yak1 *via* PKA in glucose-deprivation conditions (Martin et al. 2004). On the other hand, the relationship between TAR1 and TOR signaling in *Chlamydomonas* has not been elucidated. *vip1-1* cells accumulate higher levels of TAG than WT cells in photomixotrophic N-deficient conditions, in contrast to *tar1-1* cells, which accumulated lower levels of TAG than WT cells in TAP–N conditions. Characterization of a double mutant of *vip1* and *tar1* could reveal the relationship between TAR1 and TOR signaling and the regulatory mechanism of acetate-dependent lipid metabolism *via* TOR and/or TAR1.

In photoautotrophic conditions, why do *tar1-1* cells accumulate higher levels of starch and TAG compared with those in WT cells, although TAG and starch generally compete with each other for carbon distribution? The higher photosynthetic activity (Table 1), higher amounts of chlorophyll (Fig. 1B, 2A, B), higher expression levels of photosynthesis-related proteins (Fig. 3), and higher cell viability (Fig. 1A, 2C) in the *tar1-1* mutant contribute to the higher amounts of photosynthetic carbon products in *tar1-1* cells compared with WT cells. The fatty acid composition of TAG in *tar1-1* cells also supports the above hypothesis. The proportion of $18{:}1\Delta^{9}$ in the fatty acid composition of TAG in the *tar1-1* mutant was higher than that in WT cells (Supplementary Fig. S2). $18{:}1\Delta^{9}$ in TAG was reported to be provided mainly through *de novo* fatty acid synthesis (Riekhof et al., 2005; Li et al., 2012). On the other hand, the proportions of $18{:}3\Delta^{5,9,12}$ and $18{:}3\Delta^{9,12,15}$ in TAG in the *tar1-1* mutant were lower than those in WT cells (Supplementary Fig. S2). These polyunsaturated fatty acids

integrated into the glyceride backbone of TAG are provided from membrane lipids such as PE, DGTS MGDG, and DGDG (Sakurai et al., 2014). Considering this interpretation of the source of fatty acids in TAG, *tar1-1* cells might produce TAG using *de novo* synthesized fatty acids rather than transfer from membrane lipids. These fatty acids were possibly produced by the high photosynthetic activity in *tar1-1* cells in N-deficient conditions. Higher levels of membrane lipids remaining in *tar1-1* in TP–N conditions also support this hypothesis (Fig. 4C). Recently, another high-TAG and high-starch accumulating mutant was reported as being deficient in *malate dehydrogenase 2* (*mdh2*) (Kong et al., 2018). Kong et al. (2018) discussed the increase in TAG and starch content in the *mdh2* mutant in photoautotrophic N-deficient conditions is a combinatorial result of downregulating *β*-oxidation of fatty acids and lipolysis of TAG, enhancing their *de novo* synthesis due to increased availability of carbon precursors as well as reducing equivalent NADPH, and activation of rate-limiting enzymes of starch and fatty acids synthesis such as ADP-glucose pyrophosphorylase and acetyl-CoA carboxylase by higher levels of ROS than in WT cells. On the other hand, *tar1-1* cells produced lower levels of ROS than WT, suggesting that the high-TAG and high-starch accumulation phenotype in *tar1-1* cells is not caused by ROS-mediated activation of ADP-glucose pyrophosphorylase and acetyl-CoA carboxylase.

TAR1 regulates the induction of gametogenesis

Although the mutation in the *TAR1* gene leads to the maintenance of photosynthetic activity and cell viability even in TP−N conditions, this appears to come at a cost. Whereas in WT *C. reinhardtii*, N-deficiency is known to induce gametogenesis, which involves the differentiation of vegetative cells into sexually competent gametes (Sager and Granick 1954), we discovered that disruption of the *TAR1* gene decreased the mating efficiency of both mt^- and mt^+ gametes (Fig. 5A), as well as the accumulation of *MID* mRNA (Fig. 5B). Gene

expression analysis in *tar1-1* and WT cells indicated that TAR1 positively regulates the expression of *MID*, which is a master regulator of mt^- gametogenesis (Ferris and Goodenough 1997). In addition, the expression levels of *MTD1* and *GSM1*, which function downstream of MID (Lin and Goodenough 2007), are also positively regulated by TAR1. The expression levels of *FUS* and *SAG*, which are mt^+ gametogenic marker genes (Ferris et al. 1996, Ferris et al. 2005), are also positively regulated by TAR1. These results indicated that TAR1 is necessary for the phase transition from vegetative to gamete cells during N deficiency.

It was reported that gametes accumulate starch and degrade the cytochrome b_6/f complex in N-deficient conditions (Martin and Goodenough, 1975, Bulté and Wollman, 1992). The biological reasons of the accumulation of storage compound in gametes are speculated to be related to energy storage for the germination of zygotes, in order to survive in nutrient-limited conditions for a long period (Martin and Goodenough, 1975 and Wang et al., 2009). However, *tar1-1* showed high-starch and high-TAG accumulation and also severe inhibition of gametogenesis. Considering that normal starch accumulation occurs even in the other gametogenesis-defective mutants (Bulté and Wollman, 1992), there is no positive correlation between the efficiency of gametogenesis and accumulation of storage compounds.

TAR1 is involved in transcriptional regulation in the early phase of N-deficiency

The comparative RNA-seq analyses indicated that *TAR1* was involved in regulation to increase the mRNA abundance of genes encoding metabolic enzymes in the urea cycle, amino acid synthesis, and urate and purine transporters, both in TP−N and TAP−N conditions (Supplementary Table S2). Schmollinger et al. (2014) reported that the mRNA abundance of genes encoding the urea transporter and enzymes in the urea cycle increase in the early stage of N-deficiency in *C. reinhardtii*. They assumed that *C. reinhardtii* increases the respective gene expression to enhance the uptake of the extracellular organic nitrogen sources and to

catabolize it in response to N-deficiency. Considering their hypothesis and our transcriptomic results, TAR1 could be involved in the positive regulation of gene expression related to N-assimilation at the early phase of N-deficiency.

The mRNA abundance of 4 genes encoding tRNA ligases including *TSD2, TSV, TSW1* and putative bifunctional Glu/Pro-tRNA ligase decreased in a TAR1-dependent manner both in TP−N and TAP−N conditions (Supplementary Table S4). In keeping with this observation, the mRNA abundance of several genes encoding the other tRNA ligases increased abnormally in *tar1-1* mutant cells both in the TP−N and TAP−N conditions (Supplementary Table S3). These results suggested that TAR1 is contributive to the harmonious degradation of the cellular *de novo* protein translation apparatus in response to N-deficiency as shown previously (Park et al., 2015).

TAR1 and phospho-regulated proteins

Our phosphoproteomic analysis revealed that the GO Slim term ‘Cellular protein modification process’ was enriched among phosphoproteins whose intensities were decreased by *tar1* disruption in TP–N conditions (Fig. 7E and Supplementary Table S6). Among the phosphoproteins assigned to the protein modification process were several protein kinases related to MAPK signaling cascades (MAPK3, MAPK4, MAPK7, MAPK8, MLCK1, MEKK, and related serine/threonine protein kinases), as well as four protein phosphatases (PP2C3, PP2C4, PPP10, and PPP16). To explain these TAR1-dependent changes in phosphorylation levels, we considered the following two hypotheses: (i) the phosphorylation levels of these enzymes were maintained by TAR1; and （ii) the activity of an unknown phosphatase, which dephosphorylates these enzymes, was suppressed by TAR1-mediated protein phosphorylation in N-deficient conditions. MAPK signaling cascades are reported to play a central role in the environmental responses in the land plants (Rodriguez et al. 2010). The regulatory mechanism

between TAR1 and these TAR1-dependently phosphorylated kinases and phosphatases needs further detailed analysis.

Our phosphoproteomic analysis also identified candidate kinases that could be directly targeted by TAR1. The ion intensity of phosphopeptides derived from two protein kinases, CDPK11 and MLTK1, increased in both WT and C1 cells, but not in *tar1-1* cells. Furthermore, the identical phosphopeptides derived from CDPK11 and MLTK1 were detected in our *in vitro* phosphoproteomic analysis using recombinant TAR1 protein. *Chlamydomonas reinhardtii* CDPK11 shows 27% homology with the amino acid sequence of *A. thaliana* CDPK11. A strain of *Arabidopsis thaliana* with a mutant *CDPK11* gene exhibits an ABA insensitive phenotype (Zhu et al. 2007). Lynch et al. (2012) reported that *A. thaliana* CDPK11 interacts with AHG1 and AHG3, which are *A. thaliana* PP2C proteins belonging to subgroup A, along with ABI1. It may be possible to speculate that *C. reinhardtii* CDPK11 might interact with subgroup A PP2C members, such as PP2C3 and PPP10, downstream of TAR1-mediated protein phosphorylation.

We found that phosphopeptides derived from AMT4, GLN1, and carnosine synthase, which were detected in the *in vivo* phosphoproteomic analyses, were also detected in the *in vitro* phosphorylation assays using purified TAR1, raising the possibility that TAR1-mediated phosphorylation regulates the activities of these transporters and metabolic enzymes in N assimilation.

Recently, a *C. reinhardtii std1* mutant line, with a mutation in a plant-specific type DYRK, DYRKP, was isolated (Schulz-Raffelt et al. 2016). Similar to *tar1-1*, the *std1* mutant also accumulated higher levels of starch and TAG than WT cells, and maintained a higher photosynthetic activity in photoautotrophic CO_2-enriched (2%) and N-deficient conditions. However, several phenotypes differ between these mutants: (i) higher amounts of photosynthesis-related proteins remained in the *tar1-1* mutant than in WT cells in TP−N

conditions (Fig. 3), but many of these proteins were degraded in *std1* cells (Schulz-Raffelt et al. 2016); (ii) the amount of TAG in the *tar1-1* mutant was lower than that in WT cells in photomixotrophic N-deficient conditions (Kajikawa et al. 2015), but there were no differences between the *std1* mutant and WT cells (Schulz-Raffelt et al. 2016); (iii) *std1* cells aggregated with each other regardless of stress treatment (Schulz-Raffelt et al. 2016), but *tar1-1* cells propagated individually without cell aggregation (Supplementary Fig. S3; Kajikawa et al. 2015). Although these differences were noted, TAR1 and DYRKP may function independently to suppress photosynthetic activity and limit the accumulation of carbon stores in photoautotrophic N-deficient conditions.

Phosphoproteomic analyses revealed that TAR1 affects the phosphorylation status of a wide range of cellular processes in the initial phase of TAG-synthesis, 6 h after transfer to TP–N conditions (Fig. 8; Table 2). However, we could not deny that the result contains false positives because we have not examined the statistical significance of the results of *in vitro* assays using recombinant partial TAR1 protein. To reveal the regulatory mechanism of phosphorylation of proteins mediated by TAR1, the characterization of insertion mutants defective in factors regulated by TAR1-mediated phosphorylation protein kinases of CDPK11 and MLTK1 could reveal the biological relevance of this process to various physiological alterations in response to C/N-imbalanced stress.

Materials and Methods

Strains and culture conditions

Three *C. reinhardtii* strains including a WT strain C-9 (mt^-), an insertion mutant *tar1-1*, and the *TAR1*-complemented line (C1), have been described previously (Kajikawa et al. 2015). For photoautotrophic N-deficiency studies, cells were cultured in 50 ml Tris-phosphate (TP) culture medium (Kropat et al. 2011) supplemented with 20 mM 3-morpholinopropanesulfonic

acid (MOPS) (pH 7.2) and aeration with air containing 0.04%, 0.1%, 0.5%, 1%, 5%, or 10% CO_2 with illumination at 120 μmol photons m^{-2} s^{-1} using white fluorescent lamps. Cells in the late-logarithmic phase of growth (2.0×10^6 cells mL^{-1}) were washed twice with TP without N (TP–N) medium with 20 mM MOPS (pH 7.2), and further cultured in 50 ml TP–N medium in the same conditions for 4 days. Detailed culture conditions are described in the Supplementary Materials and Methods.

Measurements of H_2O_2 content and cell viability

The H_2O_2 concentration was measured using an Amplex™ Red Hydrogen Peroxide/Peroxidase Assay Kit (Thermo Fisher Scientific) as described by Çakmak et al. (2015). Further details are provided in Supplementary Materials and Methods. Cell viability was measured using the Evans Blue staining method, as described by Pérez-Martín et al. (2014).

Gamete induction and determination of mating efficiency

Induction of gametogenesis was performed as described previously (Lin and Goodenough 2007). Further details are provided in Supplementary Materials and Methods.

Transcriptomic and phosphoproteomic analysis

RNA-seq analysis was performed as described previously (Wang et al. 2016). Phosphoproteomic analysis was performed as described previously (Imamura et al. 2012, Choudhary et al. 2015) with minor modifications, as specified in the Supplementary Materials and Methods, as are further details of the Materials and Methods section. GO-enrichment analysis was carried out using GO Slim classification based on the annotation of *C. reinhardtii* v5.5 in Phytozome v.12 in the Blast2GO platform (Conesa et al. 2005).

Other methods

Measurement of chlorophyll content and V_{max}, immunoblotting analysis, quantification of lipid and starch, confocal and electron microscopic observations were performed as described

previously (Kajikawa et al. 2015). Anti-LHCII, anti-HemA, anti-SBP, anti-PRK, and anti-GAPDH antibodies were provided by Kentaro Ifuku (Kyoto University), Ayumi Tanaka (Hokkaido University); and Masahiro Tamoi (Kindai University), respectively.

Funding

This study was supported partly by Grants-in-Aid for Scientific Research from the Japan Society for the Promotion of Science [grant Nos. 25120714 and 16H04805 to H.F., 15K18682 to M. K. and 15H01247 to H.N.], by the Advanced Low Carbon Technology Research and Development Program of Japan Science and Technology Agency [grant No. JPMJAL1105 to H.F.], and by a Cooperative Research Grant of the Genome Research for BioResources, NODAI Genome Research Center, Tokyo University of Agriculture (H.F.).

Conflict of Interest

The authors declare that there is no conflict of interest regarding the publication of this paper.

Acknowledgements

We thank Kentaro Ifuku (Kyoto University), Yuichiro Takahashi (Okayama University), Masahiro Tamoi (Kindai University), and Ayumi Tanaka (Hokkaido University) for kindly providing the antibodies used in this analysis.

References

Anders, S. and Huber, W. (2010) Differential expression analysis for sequence count data. *Genome Biol*. 11: R106.

Aro, E.M., McCaffery, S., Anderson, J.M. (1993) Photoinhibition and D1 protein degradation in peas acclimated to different growth irradiances. *Plant Physiol*. 103: 835–843.

Baena-González, E., Rolland, F., Thevelein, J.M. and Sheen, J. (2007) A central integrator of transcription networks in plant stress and energy signalling. *Nature* 448: 938–942.

Baxter, A., Mittler, R. and Suzuki, N. (2014) ROS as key players in plant stress signalling. *J. Exp. Bot*. 65: 1229–1240.

Blaby, I.K., Blaby-Haas, C.E., Pérez-Pérez, M.E., Schmollinger, S., Fitz-Gibbon, S., Lemaire, S.D., et al. (2015) Genome-wide analysis on *Chlamydomonas reinhardtii* reveals the impact of hydrogen peroxide on protein stress responses and overlap with other stress transcriptomes. *Plant J.* 84: 974–988.

Bulté, L. and Wollman, F. A. (1992) Evidence for a selective destabilization of an integral membrane protein, the cytochrome b_6/f complex, during gametogenesis in *Chlamydomonas reinhardtii*. *Eur J Biochem*. 204: 327–336.

Çakmak, Z.E., Ölmez, T.T., Çakmak, T., Menemen,Y. and Tekinay, T. (2015) Antioxidant response of *Chlamydomonas reinhardtii* grown under different element regimes. *Phycol. Res*. 63: 202–211.

Choudhary, M.K., Nomura, Y., Wang, L., Nakagami, H. and Somers, D.E. (2015) Quantitative circadian phosphoproteomic analysis of Arabidopsis reveals extensive clock control of key components in physiological, metabolic, and signaling pathways. *Mol. Cell Proteomics*. 14: 2243–2260.

Conesa, A., Götz, S., García-Gómez, J.M., García-Gómez, J. M., Terol, J., Talón, M., et al. (2005) Blast2GO: A universal tool for annotation, visualization and analysis in functional genomics research. *Bioinformatics.* 21: 3674–3676.

Couso, I., Evans, B., Li, J., Liu, Y., Ma, F., Diamond, S., et al. (2016) Synergism between inositol polyphosphates and TOR kinase signaling in nutrient sensing, growth control and lipid metabolism in Chlamydomonas. *Plant Cell*. 28: 2026–2042.

Couso, I., Pérez-Pérez, M.E., Martínez-Force, E., Kim, H.S., He, Y., Umen, J.G., et al.(2018) Autophagic flux is required for the synthesis of triacylglycerols and ribosomal protein turnover in *Chlamydomonas*. *J. Exp. Bot.* 69: 1355–1367.

Du, Z, Lucker, B.F, Zienkiewicz, K, Miller, T.E., Zienkiewicz, A. (2018) Galactoglycerolipid lipase PGD1 is involved in thylakoid membrane remodeling in response to adverse environmental conditions in Chlamydomonas. *Plant Cell* 30: 447–465.

Fan, J., Yan, C., Andre, C., Shanklin, J., Schwender, J. and Xu, C. (2012) Oil accumulation is controlled by carbon precursor supply for fatty acid synthesis in *Chlamydomonas reinhardtii*. *Plant Cell Physiol*. 53: 1380–1390.

Ferris, P.J., Woessner, J.P. and Goodenough, U.W. (1996) A sex recognition glycoprotein is encoded by the *plus* mating-type gene *fus1* of *Chlamydomonas reinhardtii*. *Mol. Biol. Cell*. 7: 1235–1248.

Ferris, P.J. and Goodenough, U.W. (1997) Mating type in *Chlamydomonas* is specified by *mid*, the minus-dominance gene. *Genetics*. 146: 859–869.

Ferris, P.J., Waffenschmidt, S., Umen, J.G., Lin, H., Lee, J.H., Ishida, K., et al. (2005) *Plus* and *minus* sexual agglutinins from *Chlamydomonas reinhardtii*. *Plant Cell*. 17: 597–615.

Hulsmans, S., Rodriguez, M., De Coninck, B. and Rolland, F. (2016) The SnRK1 energy sensor in plant biotic interactions. *Trends Plant Sci*. 21: 648–661.

Imamura, H., Wakabayashi, M. and Ishihama, Y. (2012) Analytical strategies for shotgun phosphoproteomics: status and prospects. *Semin. Cell. Dev. Biol.* 23: 836–842.

Ishida, H., Yoshimoto, K., Izumi, M., Reisen, D., Yano, Y., Makino, A., Ohsumi, Y., Hanson, M. R., Mae, T. (2008) Mobilization of rubisco and stroma-localized fluorescent proteins of chloroplasts to the vacuole by an ATG gene-dependent autophagic process. *Plant Physiol.* 148: 142–155.

Johnson, X. and Alric, J. (2013) Central carbon metabolism and electron transport in *Chlamydomonas reinhardtii*: Metabolic constraints for carbon partitioning between oil and starch. *Eukaryot. Cell*. 12: 776–793.

Juergens, M. T., Deshpande, R. R., Lucker, B. F., Park, J. J., Wang, H., Gargouri, M. (2015) The regulation of photosynthetic structure and function during nitrogen deprivation in *Chlamydomonas reinhardtii*. *Plant Physiol*. 167: 558–573.

Juergens, M.T., Disbrow, B., Shachar-Hill, Y. (2016) The relationship of triacylglycerol and starch accumulation to carbon and energy flows during nutrient deprivation in *Chlamydomonas reinhardtii*. *Plant Physiol*. 171: 2445–2457.

Kajikawa, M., Sawaragi, Y., Shinkawa, H., Yamano, T., Ando, A., Kato, M., et al. (2015) Algal dual-specificity tyrosine phosphorylation-regulated kinase, triacylglycerol accumulation regulator1, regulates accumulation of triacylglycerol in nitrogen or sulfur deficiency. *Plant Physiol*. 168: 752–764.

Kajikawa, M., Yamauchi, M., Shinkawa, H., Tanaka, M., Hatano, K., Nishimura, Y., Kato, M., Fukuzawa, H. (2018) Isolation and characterization of *Chlamydomonas* autophagy-related mutants in nutrient-deficient conditions. *Plant Cell Physiol.* DOI: /10.1093/pcp/pcy193.

Kato, Y., Sakamoto, W. (2014) Phosphorylation of photosystem II core proteins prevents undesirable cleavage of D1 and contributes to the fine-tuned repair of photosystem II. *Plant J*. 79: 312–321.

Kong, F., Burlacot, A., Liang, Y., Legeret, B., Alseekh, S., Brotman, Y., et al. (2018) Interorganelle communication: peroxisomal MALATE DEHYDROGENASE 2 connects lipid catabolism to photosynthesis through redox coupling in Chlamydomonas. *Plant Cell* 30: 1824–1847.

Kropat, J., Hong-Hermesdorf, A., Casero, D., Ent, P., Castruita, M., Pellegrini, M., et al. (2011) A revised mineral nutrient supplement increases biomass and growth rate in *Chlamydomonas reinhardtii*. *Plant J.* 66: 770–780.

Li, X., Moellering, E.R., Liu, B., Johnny, C., Fedewa, M., Sears, B.B., et al. (2012) A galactoglycerolipid lipase is required for triacylglycerol accumulation and survival following nitrogen deprivation in *Chlamydomonas reinhardtii*. *Plant Cell*. 24: 4670–4686.

Lin, H. and Goodenough, U.W. (2007) Gametogenesis in the *Chlamydomonas reinhardtii minus* mating type is controlled by two genes, *MID* and *MTD1*. *Genetics.* 176: 913–925.

Lynch, T., Erickson, B.J. and Finkelstein, R.R. (2012) Direct interactions of ABA-insensitive(ABI)-clade protein phosphatase(PP)2Cs with calcium-dependent protein kinases and ABA response element-binding bZIPs may contribute to turning off ABA response. *Plant Mol. Biol*. 80: 647–658.

Martin, N. C., and U. W. Goodenough. (1975) Gametic differentiation in *Chlamydomonas reinhardtii*. I. Production of gametes and their fine structure. *J. Cell Biol.* 67:587–605.

Martin, D.E., Soulard, A. and Hall, M.N. (2004) TOR regulates ribosomal protein gene expression via PKA and the forkhead transcription factor FHL1. *Cell* 119: 969–979.

Merchant, S.S., Kropat, J., Liu, B., Shaw, J. and Warakanont, J. (2012) TAG, You're it! Chlamydomonas as a reference organism for understanding algal triacylglycerol accumulation. *Curr. Opin. Biotechnol*. 23: 352–363.

Moriya, H., Shimizu-Yoshida, Y., Omori, A., Iwashita, S., Katoh, M. and Sakai, A. (2001) Yak1p, a DYRK family kinase, translocates to the nucleus and phosphorylates yeast Pop2p in response to a glucose signal. *Genes Dev.* 15: 1217–1228.

Park, J.J., Wang, H., Gargouri, M., Deshpande, R.R., Skepper, J.M., Holguin, O., et al. (2015) The response of *Chlamydomonas reinhardtii* to nitrogen deprivation: a systems biology analysis. *Plant J.* 81: 611–624.

Pérez-Martín M, Pérez-Pérez M.E., Lemaire S.D. and Crespo J.L. (2014) Oxidative stress contributes to autophagy induction in response to endoplasmic reticulum stress in *Chlamydomonas reinhardtii*. *Plant Physiol*. 166: 997–1008.

Pérez-Pérez, M.E., Lemaire, S.D. and Crespo, J.L. (2012) Reactive oxygen species and autophagy in plants and algae. *Plant Physiol.* 160: 156–164.

Plumley, F.G., Schmidt, G.W. (1989) Nitrogen-dependent regulation of photosynthetic gene expression. *Proc. Natl. Acad. Sci. USA* 86: 2678–2682.

Riekhof., W.R., Sears, B.B., Benning, C. (2005) Annotation of genes involved in glycerolipid biosynthesis in *Chlamydomonas reinhardtii*: Discovery of the betaine lipid synthase $BTA1_{Cr}$. *Eukaryot. Cell* 4: 242–252.

Rodriguez, M.C.S., Petersen, M. and Mundy, J. (2010) Mitogen-activated protein kinase signaling in plants. *Annu. Rev. Plant Biol*. 61: 621–649.

Roustan, V., Bakhtiari, S., Roustan, P.J. and Weckwerth, W. (2017) Quantitative in vivo phosphoproteomics reveals reversible signaling processes during nitrogen starvation and recovery in the biofuel model organism *Chlamydomonas reinhardtii*. *Biotechnol. Biofuels.* 10: 1–24.

Sager, R. and Granick, S. (1954) Nutritional control of sexuality in *Chlamydomonas reinhardi*. *J. Gen. Physiol*. 65: 729–742.

Sakurai, K., Moriyama, T. and Sato, N. (2014) Detailed identification of fatty acid isomers sheds light on the probable precursors of triacylglycerol accumulation in photoautotrophically grown *Chlamydomonas reinhardtii*. *Eukaryot. Cell* 13: 256–266.

Sarkar, N., Lemaire, S., Wu-Scharf, D., Issakidis-Bourguet, E. and Cerutti, H. (2005) Functional specialization of *Chlamydomonas reinhardtii* cytosolic thioredoxin h1 in the response to alkylation-induced DNA damage. *Eukaryot. Cell* 4: 262–273.

Schmollinger, S., Mühlhaus, T., Boyle, N.R., Blaby, I.K., Casero, D., Mettler, T. et al. (2014) Nitrogen-sparing mechanisms in *Chlamydomonas* affect the transcriptome, the proteome, and photosynthetic metabolism. *Plant Cell* 26: 1410–1435.

Schulz-Raffelt, M., Chochois, V., Auroy, P., Cuiné, S., Billon, E., Dauvillée, D. et al. (2016) Hyper-accumulation of starch and oil in a *Chlamydomonas* mutant affected in a plant-specific DYRK kinase. *Biotechnol. Biofuels.* 9: 55.

Shao, N., Duan, G.Y. and Bock, R. (2013) A mediator of singlet oxygen responses in *Chlamydomonas reinhardtii* and *Arabidopsis* identified by a luciferase-based genetic screen in algal cells. *Plant Cell.* 25: 4209–4226.

Shashkova, S., Welkenhuysen, N. and Hohmann, S. (2015) Molecular communication: crosstalk between the Snf1 and other signaling pathways. *FEMS Yeast Res*. 15: 1–10.

Siaut, M., Cuiné, S., Cagnon, C., Fessle, B., Nguyen, M., Carrier, P. et al. (2011) Oil accumulation in the model green alga *Chlamydomonas reinhardtii*: characterization, variability between common laboratory strains and relationship with starch reserves. *BMC Biotechnol*. 11: 7.

Tikkanen, M. and Aro, E.M. (2012) Thylakoid protein phosphorylation in dynamic regulation of photosystem II in higher plants. *Biochim. Biophys. Acta-Bioenerg.* 1817: 232–238.

Wang, Z.T., Ullrich, N., Joo, S., Waffenschmidt, S. and Goodenough, U. (2009) Algal lipid bodies: stress induction, purification, and biochemical characterization in wild-type and starchless *Chlamydomonas reinhardtii*. *Eukaryot*. *Cell* 8: 1856–1868.

Wang, L., Yamano, T., Takane, S., Niikawa, Y., Toyokawa, C., Ozawa, S., et al. (2016) Chloroplast-mediated regulation of CO_2-concentrating mechanism by Ca^{2+}-binding protein CAS in the green alga *Chlamydomonas reinhardtii*. *Proc. Natl. Acad. Sci*. *USA* 113: 12586–12591.

Wei, L., Derrien, B., Gautier, A., Houille-Vernes, L., Boulouis, A., Saint-Marcoux, D. et al. (2014) Nitric oxide-triggered remodeling of chloroplast bioenergetics and thylakoid proteins upon nitrogen starvation in *Chlamydomonas reinhardtii. Plant Cell* 26: 1–21.

Zhu, S.Y., Yu, X.C., Wang, X.J., Zhao, R., Li, Y., Fan, R.C. et al. (2007) Two calcium-dependent protein kinases, CPK4 and CPK11, regulate abscisic acid signal transduction in *Arabidopsis*. *Plant Cell* 19: 3019–3036.

Table 1. Photosynthetic characteristics of wild-type (WT), *tar1-1*, and complementation line (C1) cells in photoautotrophic N-deficient conditions.

Parameter	Strain	Time after transfer to TP–N conditions (days)			
		0	**1**	**2**	**4**
Maximum quantum yield (F_V/F_m) of PS-II	WT	0.72 ± 0.01	0.27 ± 0.03	UD	UD
	tar1-1	0.72 ± 0.01	0.49 ± 0.02*	0.27 ± 0.13	0.04 ± 0.03
	C1	0.70 ± 0.03	0.22 ± 0.03	UD	UD
Quantum efficiency (ΦII) of PS-II	WT	0.65 ± 0.00	0.16 ± 0.02	UD	UD
	tar1-1	0.65 ± 0.00	0.31 ± 0.03*	0.09 ± 0.08	UD
	C1	0.61 ± 0.00	0.17 ± 0.05	UD	UD
Maximum photosynthetic rates of O_2-evolution (μmol O_2 mg Chl^{-1} h^{-1})	WT	294 ± 7	10 ± 2	UD	UD
	tar1-1	266 ± 11*	213 ± 4*	72.4 ± 12*	UD
	C1	281 ± 7	24 ± 2	UD	UD

Cells cultured photoautotrophically in Tris-acetate-phosphate culture medium aerated with air containing 5% CO_2 were transferred to Tris-phosphate medium without an N source, and aerated with air containing 5% CO_2 (TP–N). Data in all experiments indicate mean value ± standard deviation from three biological replicates. Significant differences (*$p < 0.05$) compared with WT cells were determined using Student's *t* test. Chl, chlorophyll; PS-II, photosystem II; UD, undetectable.

Table 2. Candidate phosphorylation substrates for TAR1.

	Protein name	Gene name	Peak group ID	Phosphosites	Description
Kinase					
	Cre06.g310100	MLTK1	3232	S350, S351	Mitogen-activated protein kinase kinase kinase
	Cre13.g564500	CDPK11	3805	T655	Ca^{2+}/calmodulin-dependent protein kinase, EF-hand protein superfamily
RNA polymerase					
	Cre16.g673900	RPC3	392	S359, S362	DNA-directed RNA polymerase III subunit RPC3 (RPC3, POLR3C)
N assimilation and carbon metabolic process					
	Cre02.g113200	GLN1	2823	S54	Glutamine synthetase
	Cre06.g262900	PFK1	4316	S77, S81	Phosphofructokinase
	Cre13.g569850	AMT4	3708	S475	Ammonium transporter. Belongs to AMT1 family (AMT1;4 or AMT1.4)
	Cre13.g582800		1736, 1188	S135, S155	Carnosine synthase
Stress response					
	Cre03.g177500		611	S166	Receptor expression-enhancing protein 5/6 (REEP5_6)
	Cre16.g663000	PRX	3598	S424	Thioredoxin peroxidase
Others					
	Cre01.g004400		2909	S126	
	Cre03.g180450	FAP215	216, 2489	S60, S578	5'-Nucleotidase and flagellar associated protein
	Cre10.g447950		574, 4153	S67, S70	
	Cre10.g467000	IFT57	1229	S464	Intraflagellar transport protein 57
	Cre14.g614850	FAP33	2552	S1069	Flagellar associated protein
	Cre14.g624900	FAP171	3814	S675	Predicted integral membrane protein
	Cre16.g689423		3406	S88	Flagellar associated protein
	Cre16.g691440	FAP43	5181	S655	
	Cre17.g706600		3006	T162	

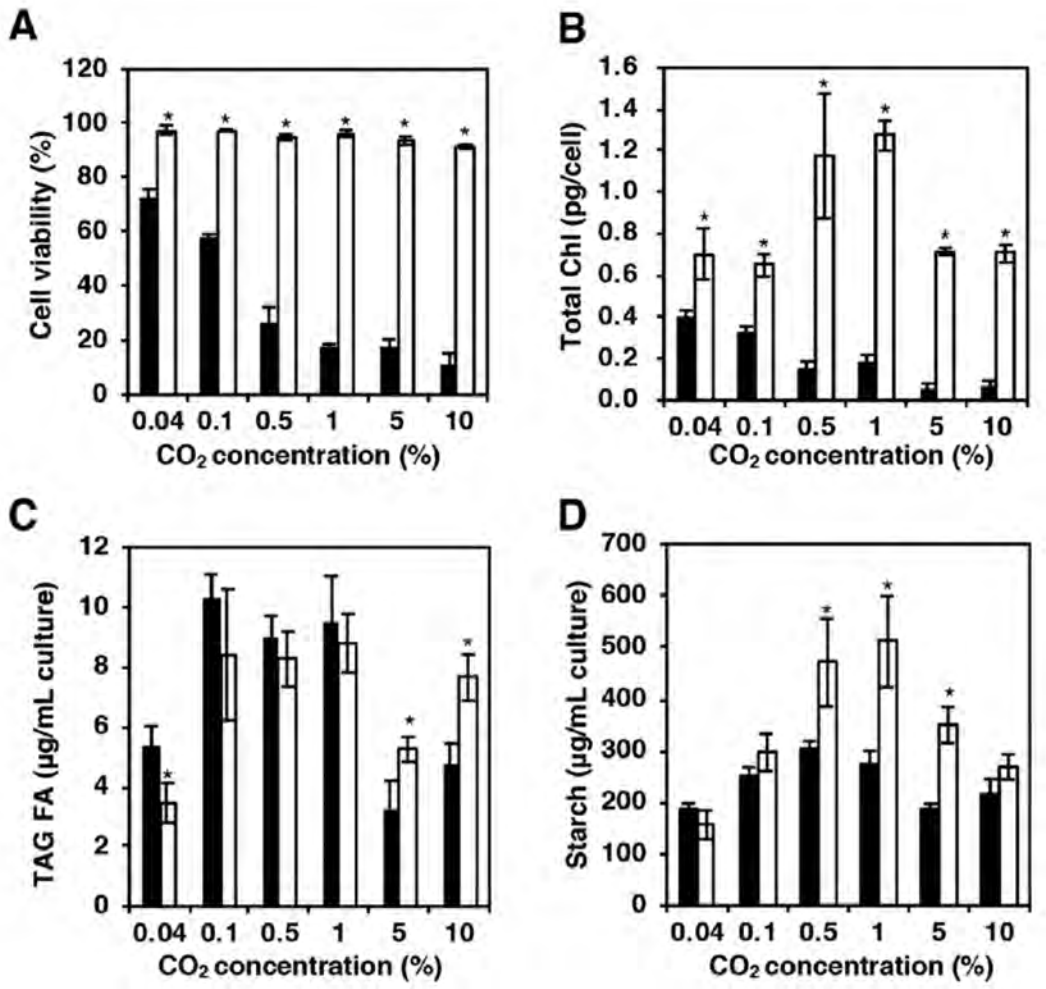

Figure 1. CO_2-dependent cell viability (A) and accumulation of chlorophyll per cell (B), fatty acids (FA) in triacylglycerol (TAG) (C), and starch (D) in wild-type (WT; closed box) and *tar1-1* (open box) cells in photoautotrophic N-deficient conditions. After transfer to photoautotrophic N-deficient conditions, cell cultures were aerated with air containing 0.04% (ambient), 0.1%, 0.5%, 1%, 5%, or 10% CO_2 for 2 days. Levels of TAG FA and starch are expressed per culture volume. Data indicate mean values ± SD from three biological replicates. Asterisks denote statistically significant differences compared with WT cells using Student's *t* test (*$p < 0.05$).

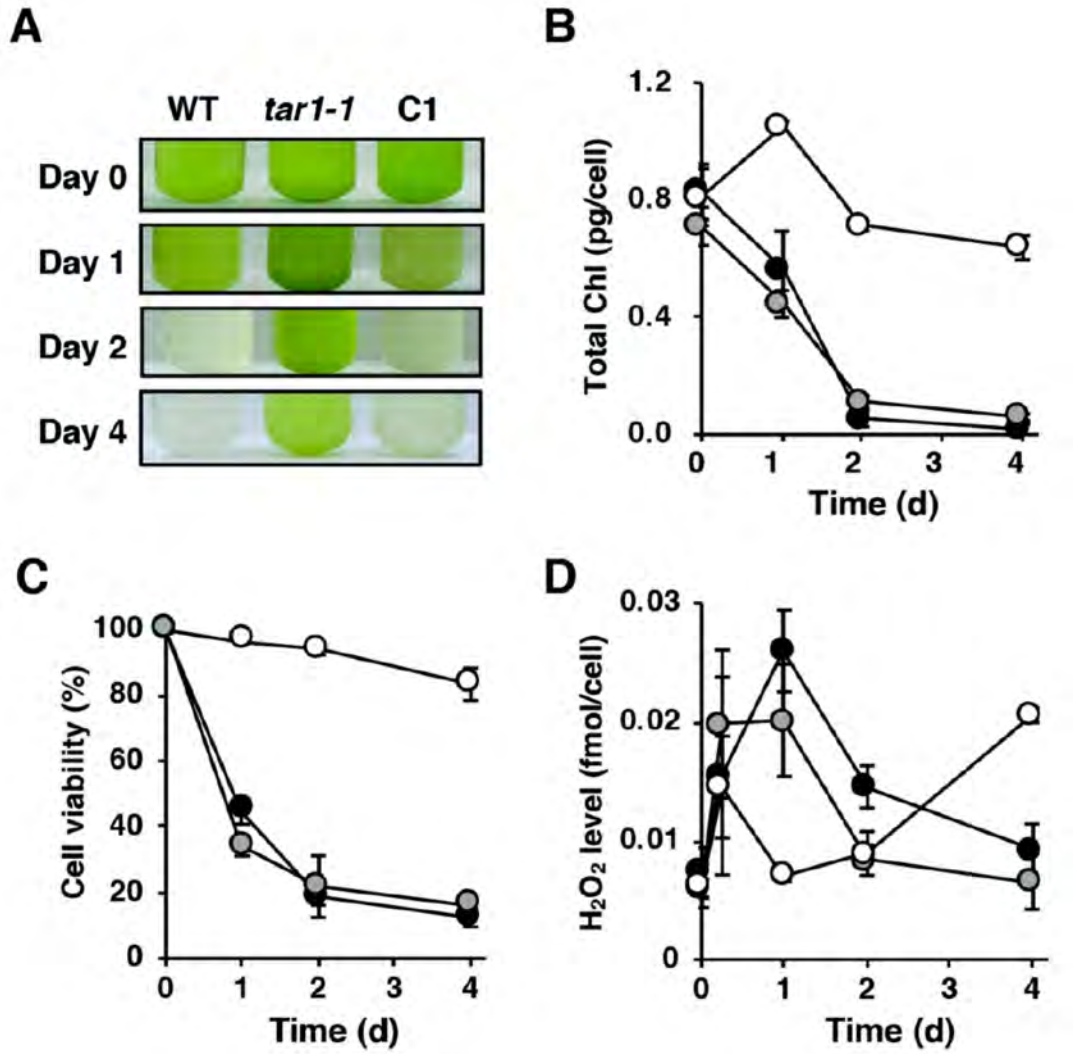

Figure 2. Stress responses of *tar1-1* cells to nitrogen (N)-deficiency.

(A) Images of cultures of wild-type (WT), *tar1-1*, and complementation line (C1) cells after transfer to photoautotrophic N-deficient conditions with aeration with air containing 5% CO_2 (TP−N). (B) chlorophyll content, (C) cell viability and (D) H_2O_2 content of WT (closed circle), *tar1-1* (open circle), and C1 (gray circle) cells after transfer to TP–N conditions aerated with air containing 5% CO_2. Data indicate mean values ± SD from three biological replicates.

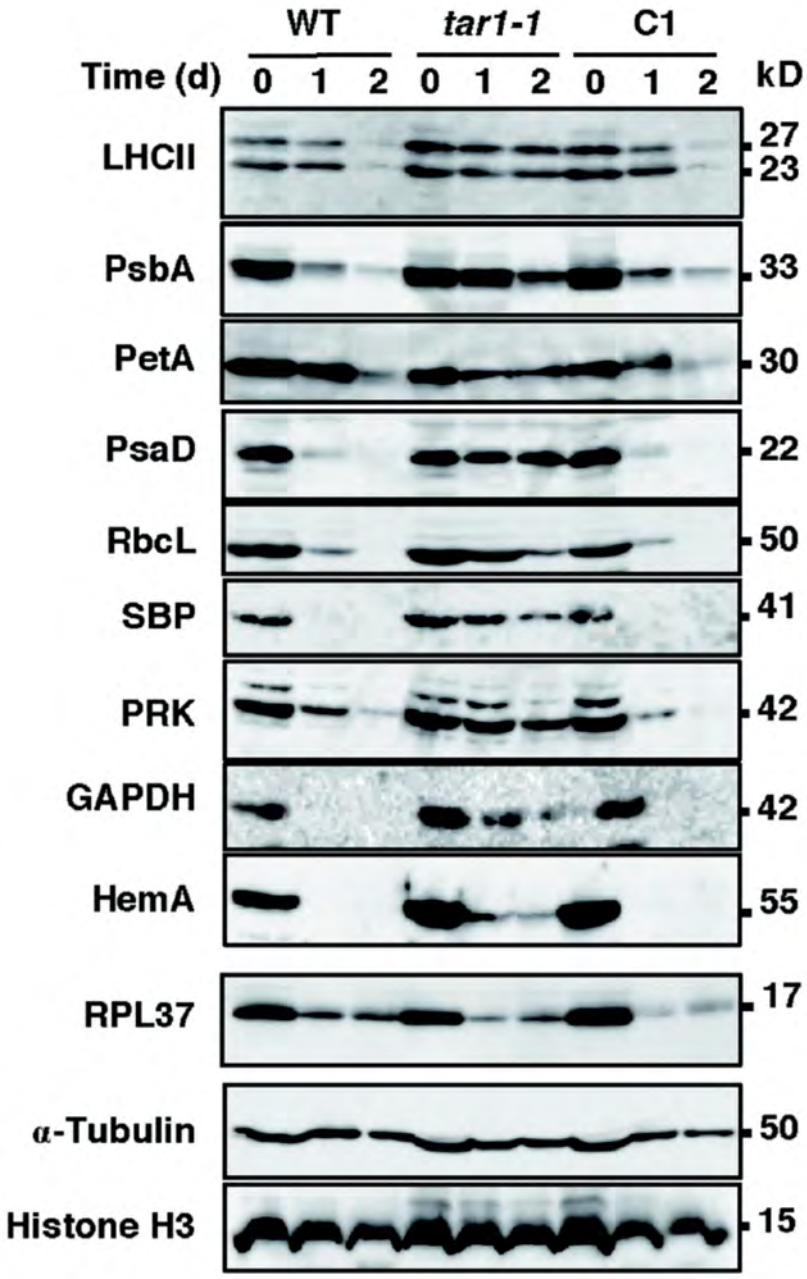

Figure 3. Immunoblotting analysis of photosynthesis-related proteins in wild-type (WT), *tar1-1*, and complementation line (C1) cells after transfer to photoautotrophic nitrogen (N)-deficient conditions with aeration with air containing 5% CO_2 (TP−N). Antibodies against light-harvesting complex protein II (LHCII) in antenna, D1 protein in PSII (PsbA), cytochrome *f* in the cytochrome b_6/*f* complex (PetA), the subunit II protein in PSI (PsaD), proteins related to the Calvin–Benson cycle including the large subunit of Rubisco (RbcL), sedoheptulose-1,7-bisphosphate (SBP), phosphoribulokinase (PRK), and glyceraldehyde-3-phosphate dehydrogenase (GAPDH), chloroplastic glutamyl-tRNA reductase 1 (HemA) for chlorophyll biosynthesis, and cytoplasmic ribosomal protein (RPL37) were used for immunoblotting, along with loading controls (*α*-tubulin and histone H3).

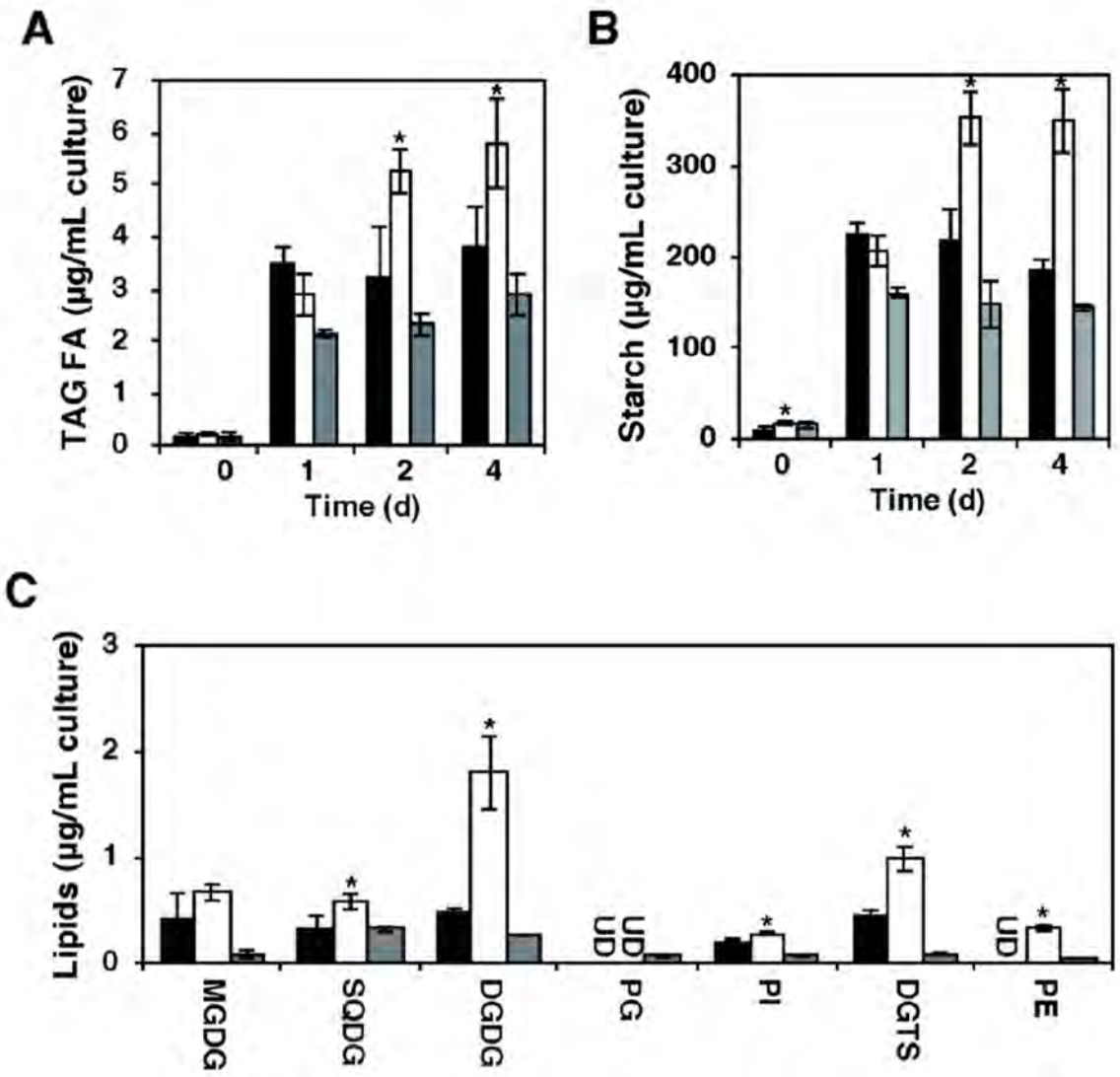

Figure 4. Accumulation of fatty acids (FAs) in triacylglycerol (TAG) (A), starch (B), and major polar lipid classes (C) in *C. reinhardtii* cells after transfer to photoautotrophic nitrogen (N)-deficient cultures with aeration with air containing 5% CO_2 (TP−N). Wild-type, a mutant *tar1-1,* and complementation line C1 are indicated by closed, open and gray boxes, respectively. Lipid classes were analyzed at 2 day. DGDG, digalactosyldiacylglycerol; DGTS, diacylglycerol-*N*, *N*, *N*-trimethylhomoserine; MGDG, monogalactosyldiacylglycerol; PE, phosphatidylethanolamine; PG, phosphatidylglycerol; PI, phosphatidylinositol; SQDG, sulfoquinovosyldiacylglycerol. UD; undetectable. Data indicate mean value ± SD from three biological replicates. Asterisks indicate statistically significant differences compared with WT using Student's *t* test (*$p < 0.05$).

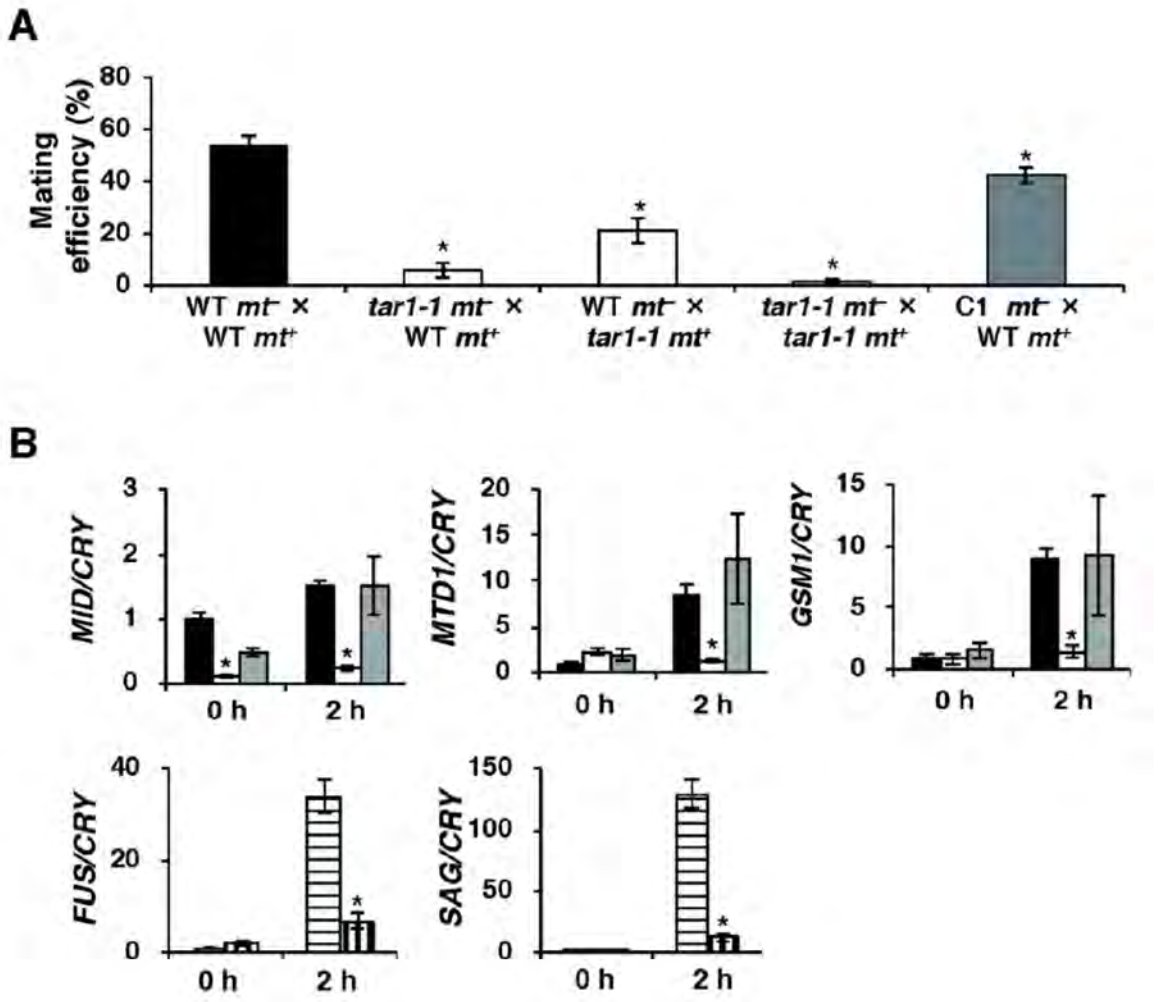

Figure 5. Effect of *TAR1* mutation on gamete induction.

(A) The mating efficiency after mixing of gamete-induced wild-type (WT), *tar1-1*, and complemented line (C1) cells with different combinations of mating types. (B) Relative mRNA abundance of gamete-specific genes in gametes of WT (C9, mt^-) (filled box), *tar1-1* (mt^-) (open box), C1 (mt^-) (gray box), WT (CC-125, mt^+) (horizontal striped bar), and *tar1-1*-F2-11 (mt^+) (vertical striped bar) cells deduced by quantitative real-time PCR. RNA samples were isolated from cells cultured in high-salt minimal medium without a nitrogen to induce gametogenesis. Data indicate mean value ± SD from three biological replicates. Asterisks indicate statistically significant differences compared with the WT using Student's *t* test (*$p < 0.05$).

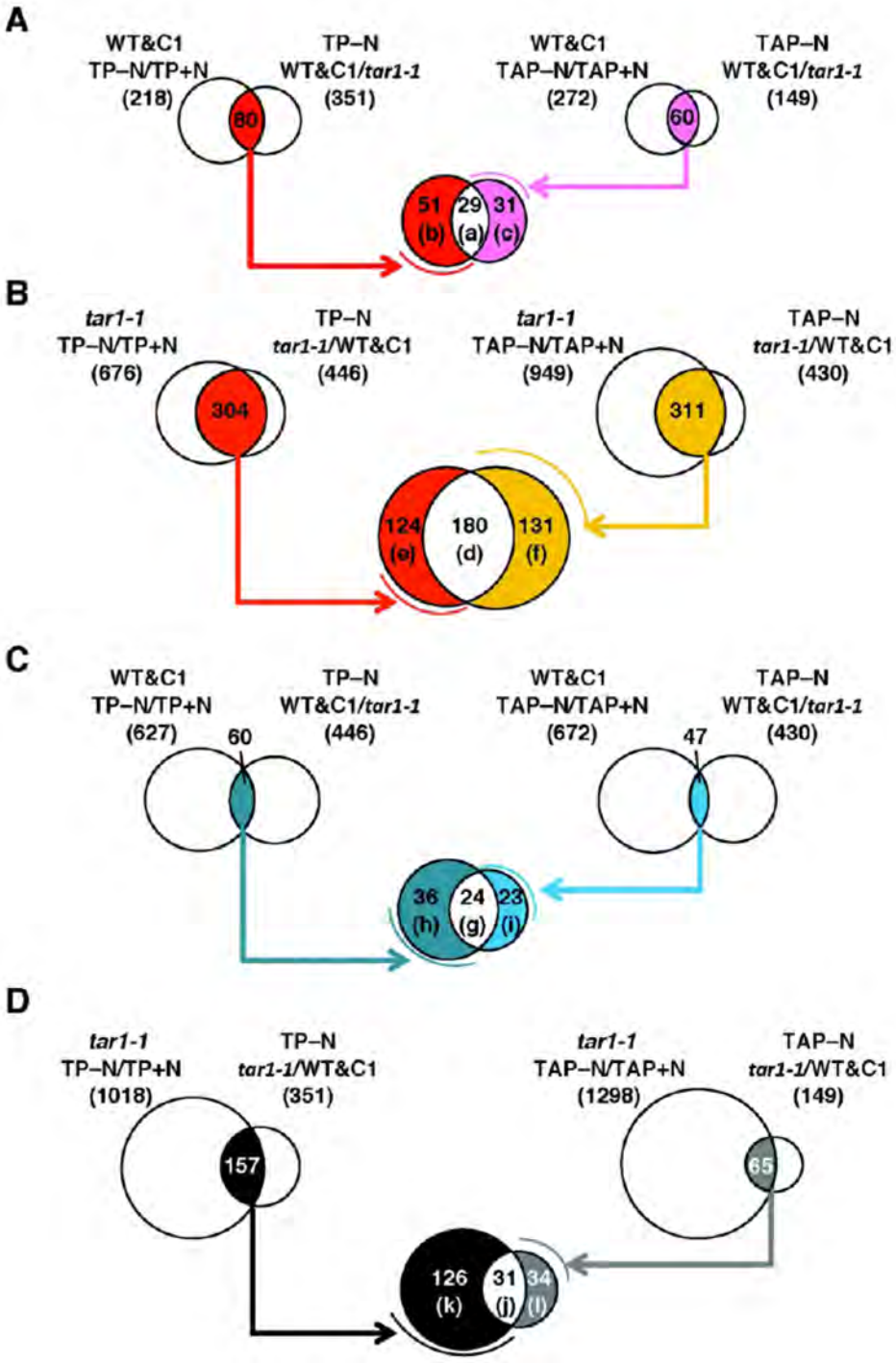

Figure 6. Venn diagrams indicating differentially expressed genes (DEGs) in wild-type (WT), *tar1-1*, and complementation line (C1) cells after 6 h in photoautotrophic nitrogen (N)-deficient conditions aerated with air containing 5% CO_2 (TP–N) or photomixotrophic N-deficient conditions (TAP–N; Kajikawa et al., 2015) compared with the corresponding N replete conditions, respectively. Numbers of DEGs which are significantly changed between culture conditions or among strains are shown in parentheses. Genes in each group are listed in Supplementary Dataset S3-S14 as follows: (A) DEGs whose expression levels were up-regulated *TAR1*-dependently in common in N-deficient conditions (group a, Supplementary Dataset S3) with TP–N (group b, Supplementary Dataset S4) or TAP–N (group c, Supplementary Dataset S5). (B) DEGs whose expression levels were increase by *tar1* disruption in common in N-deficient conditions (group d, Supplementary Dataset S6) or with TP–N (group e, Supplementary Dataset S7) or TAP–N (group f, Supplementary Dataset S8). (C) DEGs whose expression levels were down-regulated *TAR1*-dependently in common in N-deficient conditions (group g, Supplementary Dataset S9) with TP–N (group h, Supplementary Dataset S10) or TAP–N (group i, Supplementary Dataset S11). (D) DEGs whose expression levels were decrease by *tar1* disruption in common in N-deficient conditions (group j, Supplementary Dataset S12) with TP–N (group k, Supplementary Dataset S13) or TAP–N (group l, Supplementary Dataset S14).

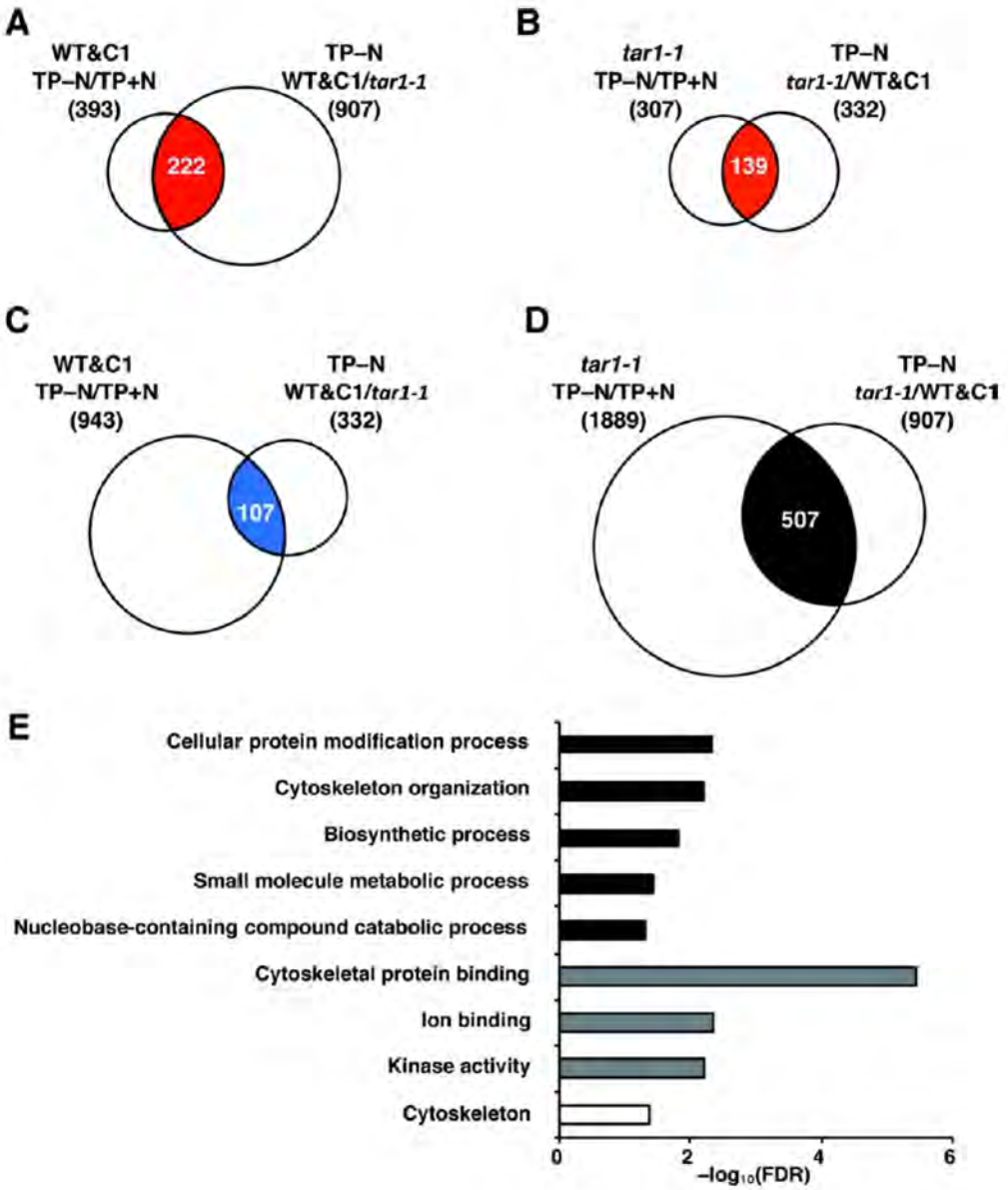

Figure 7. Comparative phosphoproteomic analyses of wild-type (WT), *tar1-1*, and complementation line (C1) cells after 6 h in photoautotrophic nitrogen (N)-deficient conditions aerated with air containing 5% CO_2 (TP–N). Venn diagram indicating phosphopeptides whose intensities increased or decreased significantly in WT, *tar1-1*, and C1 cells after 6 h in TP–N, compared with photoautotrophic N-replete conditions. Numbers of phosphopeptides which are significantly changed between culture conditions or among strains are shown in parentheses. Phosphopeptides in each group are listed in Supplementary Dataset S17-S20 as follows: (A) Phosphopeptides whose intensities were up-regulated TAR1-dependently in TP–N conditions (Supplementary Dataset S17). (B) Phosphopeptides whose intensities were increased by *tar1*-disruption in TP–N conditions (Supplementary Dataset S18). (C) Phosphopeptides whose intensities were down-regulated TAR1-dependently in TP–N conditions (Supplementary Dataset S19). (D) Phosphopeptides whose intensities were decreased by *tar1*-disruption in TP–N condition (Supplementary Dataset S20). (E) GO classification and statistical analysis of phosphoproteins in D (Supplementary Table S6) by Blast2GO. Bar charts for functional categories of biological process (closed box), molecular functions (gray box) and cellular component (open box). The Y-axis exhibits representative enriched GO Slim terms. The X-axis shows the $-LOG_{10}$ (false discovery rate, FDR).

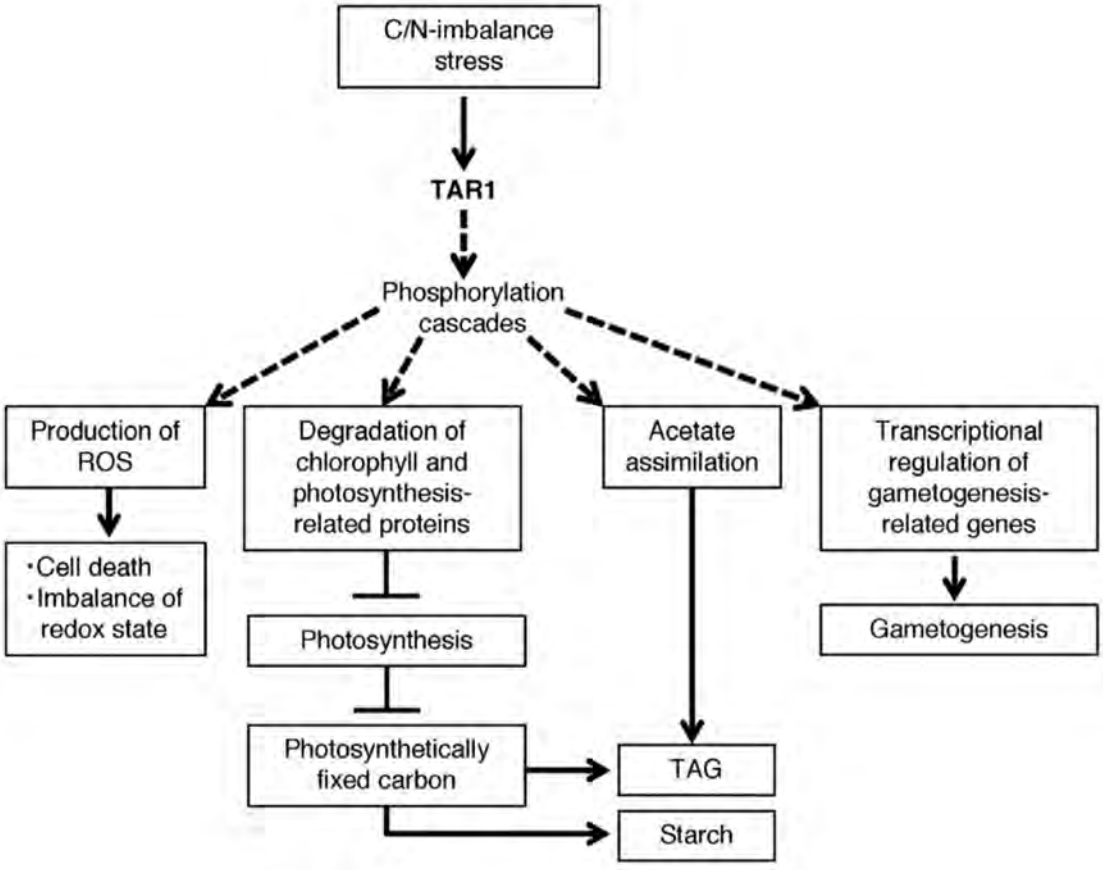

Figure 8. Hypothetical model of the functional roles of TAR1 in cellular responses to carbon (C)/nitrogen (N)-imbalance stress. Possible protein phosphorylation-mediated steps are indicated by broken arrows. ROS, reactive oxygen species.